CFD ANALYSIS OF THE HEAVY LIQUID METAL FLOW FIELD IN THE MYRRHA POOL

Ferry Roelofs, Ed Komen

NRG, Westerduinweg 3, PO Box 25, 1755 ZG Petten, The Netherlands

Katrien Van Tichelen, Peter Kupschus, Hamid Aït Abderrahim SCK •CEN, Boeretang 200, 2400 Mol, Belgium, myrrha@sckcen.be

Abstract

SCK CEN, the Belgian Nuclear Research Centre, is designing an accelerator-driven system (ADS), MYRRHA, which aims to serve as a basis for the European experimental ADS and to provide protons and neutrons for various R&D applications. It consists of a proton accelerator that delivers a 350 MeV, 5 mA proton beam to a liquid lead-bismuth eutectic (LBE) spallation target, which in turn couples to an LBE-cooled, subcritical fast-spectrum core in a pool-type configuration. The liquid metal flow pattern in the lower part of the MYRRHA pool vessel needs to be investigated in order to assess the details of recirculation and stagnant zones for adequate coolant flow and sufficient physico-chemical mixing as well as to judge the scaling of flow down to a model that can be handled experimentally. To this end, three-dimensional (3-D) computational fluid dynamics calculations were performed by NRG in collaboration with the MYRRHA team.

Introduction

The subcritical core of the MYRRHA ADS is submerged in a pool filled with LBE, which serves as a coolant and neutron reflector medium (see Figure 1 [1]). The ~60 m³ of LBE fills a vessel of roughly 4 m inner diameter and 6 m height. Under full operational conditions, the LBE is "cold" at ~200 C in the lower part and flows through the central core upwards being heated to ~350°C on average. This "hot" zone is separated by a diaphragm from the "cold" zone. Four eccentrically positioned pumps force the circulating flow downwards through heat exchangers and provide the pressure head for core cooling.

Since the cold zone or lower pool is spacious enough to permit the loading of the core and the exchange of fuel, it is necessary to gain knowledge about the behaviour of the flow pattern in the lower part of the pool with emphasis on the occurrence of recirculation and stagnant zones. Such features could influence the cooling or the physico-chemistry of the LBE that is corrosive to the steel used. The latter will be protected by proper dynamic oxygen control of the LBE whose concentration may not be controllable if sufficient mixing is not allowed. The objective of the present analyses is to evaluate the basic isothermal flow pattern in the lower part of the vessel in order to assess the presence of recirculation and stagnant zones for the full-size device in normal and abnormal operating conditions. The CFD analyses will be extended later on to cases where hot injection takes place and finally the full thermal cycle may be modelled.

Although the CFD results will be used as a guideline, experiments are still necessary but are not economically possible at the scale of the foreseen device. Therefore, the lower part of the MYRRHA pool vessel needs to be scaled down by a linear factor of up to 10, which would allow for the building of a model containing 60 l instead of 60 m³ of LBE. The second objective of the present analysis is to evaluate the influence on flow topology of the downscaling of the MYRRHA pool by a factor of up to 10. To this end, a scaling method preserving the relevant flow features should be defined.

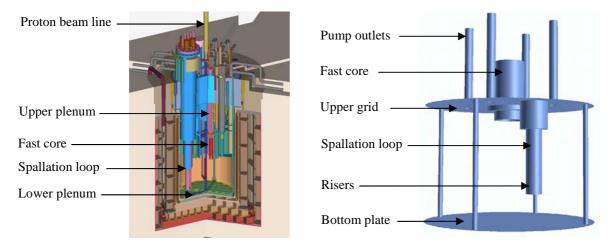


Figure 1. The MYRRHA ADS and its lower pool model

Geometry of the lower MYRRHA pool

The lower pool space of MYRRHA to be modelled is a cylindrical space of 4 m inner diameter and height of ~2 m (see Figure 1). The bottom surface is covered by a unit that provides electrical heating and process gas injection for oxygen control. Neither of the functions is relevant here but the

surface roughness of this structure was taken into account. The same is true for the top boundary, which consists of a grid to prevent detached objects from floating into trapping spaces of the diaphragm. The lower pool unit hangs from the diaphragm, and the four support stanchions for pump and heat exchanger units are to be modelled in case they present obstacles to azimuthally developing flow by virtue of pump imbalances. A further asymmetric obstacle is introduced by the spallation loop. The coupling between the spallation loop and the lower pool through the spallation loop heat exchanger was not modelled. The inlet mass flow rate of the injecting pumps was taken as 350 kg/s for each injecting pump through a nozzle of 200 mm in diameter.

Scaling methods

The turbulent jets leaving the four pump units determine the flow pattern. Three different scaling methods were considered based on varying importance of the physical parameters characterising a jet:

- The turbulent jet is characterised by the Reynolds number with the pool diameter at characteristic length. In this case, the jets emerging from the down-scaled nozzles were equivalent to the jets emerging from the original nozzle when the velocity is increased (*Reynolds number*).
- The time a jet needs to reach the bottom of the MYRRHA pool is considered characteristic for the jet. The inlet velocity was scaled by the same factor as the geometry (*characteristic time*).
- The velocity of the jet at the pump outlet characterises the jet. At the same time, the volume throughput time was kept constant (*inlet velocity*).

The three methods are summarised in Table 1. The correct choice for the scaling method is not obvious and depends on the phenomena investigated. In the case of physico-chemistry effects, timescales are most important and emphasis will be put on the correct representation of residence times.

Table 1. Scaling methods (geometric scaling factor f)

Scaling method	Inlet diameter [m]	Pool diameter [m]	Inlet area [m²]	Pool volume [m³]	Volume flow [m³/s]	Inlet velocity [m/s]	Through -put time [s]	Reynolds number
Reynolds	1/f	1/f	1/f2	$1/f^3$	1/f	f	1/f2	1
Characteristic time	1/f	1/f	1/f ²	1/f ³	$1/f^3$	1/f	1	1/f ²
Inlet velocity	$1/f^{3/2}$	1/f	$1/f^3$	$1/f^3$	1/f ³	1	1	1/f

In order to compare results obtained with various scaling methods, a dimensionless velocity and a dimensionless residence time are defined. The dimensionless velocity ($v \not \phi$ was obtained by dividing the velocity (v) by the inlet velocity (v_{inlet}):

$$v' = \frac{v}{v_{inlet}} \,.$$

The inlet velocity was obtained from the specified mass flow rate at the pump outlets, the pump outlet area and the density of the applied fluid. The dimensionless residence time ($t \zeta_{es}$) was obtained by dividing the residence time (t_{res}) by a characteristic time:

$$t'_{res} = \frac{t_{res}}{D_{pool} / \left(C \frac{f_{v}}{A_{pool}}\right)}$$

where D_{pool} is the diameter of the pool, f_v is the volume flow and A_{pool} is the area of a horizontal cut-plane of the pool. C equals:

$$C = \frac{A_{pool, fullscale}}{A_{inlet, fullscale}}$$

where $A_{pool, full \ scale}$ is the area of the full-scale pool and $A_{inlet, full \ scale}$ is the area of a full scale inlet.

Cases

The flow topology was analysed for various scenarios, with special emphasis on the presence of stagnant zones. In the Base Case scenario, all four pumps had equal performance. For Cases 1a through 1f, one or two pumps were stopped with no throughput permitted; the other pumps had equal performances per pump as compared to the Base Case. This is operationally not correct since the flow rates of the operating pumps would be increased. However, these results will provide the design team with useful information about the residence times for each scenario.

The main dimensions of the pool were scaled down by a factor of five for the Cases 2a, 2b and 2c. Scaling was based on the Reynolds number, characteristic time and velocity, respectively. The model was scaled down by a factor of 10 for Case 3. In this analysis, scaling based on characteristic time was used. The cases are summarised in Table 2.

Table 2. Cases

Case	Case description
Base	No pump tripping and no scaling
1a	Full scale, 1 pump close to the spallation loop tripped
1b	Full scale, 1 pump opposite the spallation loop tripped
1c	Full scale, 2 pumps close to the spallation loop tripped
1d	Full scale, 2 pumps opposite the spallation loop tripped
1e	Full scale, 1 pump close to the spallation loop and 1 pump opposite
	the spallation loop, but close to the first pump, tripped
1f	Full scale, 1 pump close to the spallation loop and 1 pump opposite
	the spallation loop, but diagonally opposite to the first pump, tripped
2a	Scaled down by a factor of 5, scaling based on Reynolds number
2b	Scaled down by a factor of 5, scaling based on characteristic time
2c	Scaled down by a factor of 5, scaling based on velocity
3	Scaled down by a factor of 10, scaling based on characteristic time

CFD calculations

CFD model

Computer code

The computations were performed using the widely used commercial CFD code, CFX5.5 [1].

Mesh

The mesh for the lower MYRRHA pool model consisted of 911 000 hexahedral computational cells. The k-e turbulence model in combination with scalable wall functions as implemented in CFX5 was selected for the current analyses. Therefore, the mesh refinement near the walls should ideally be such that the non-dimensionless distance y^+ is larger than 12 in order to model the boundary layers. However, the wall friction was predicted with sufficient accuracy for this application, even for lower values of y^+ [1]. For the full-scale model, the values of y^+ were in the range of 20 to 200. For the scaled-down model, the values of y^+ were in the range of 4 to 20.

Main fluid dynamics model

The main fluid dynamics model describes a single phase steady-state time-averaged incompressible turbulent flow. The k-e turbulence model in combination with scalable wall functions as implemented in CFX5 [2] was selected to model turbulence. The MYRRHA core was modelled by a porous medium, such that the pressure drop over the core is in accordance with the actual pressure drop of 3 bar [4] although this may cause a non-physical velocity profile at the core entrance, which must be considered with some prudence. The influence is negligible, however, of the velocity profile at the core entrance for the location where the maximum residence time occurs.

Properties

For the density and the dynamic viscosity of liquid lead-bismuth, constant properties were used at a temperature of 200 C as obtained from [1].

Boundary conditions

At the outlets of the pump sections, the mass flow rate (350 kg/s per pump), the turbulence intensity (5%) and the turbulent length scale (0.02 m) were specified. Based on user experience, it was concluded that the selection of the latter two quantities has no effect on the computed flow field. At the outlet of the MYRRHA core, the static pressure was prescribed, whereas zero normal gradients were used for all remaining flow variables.

In the full-scale model, at the lower and upper plates of the lower MYRRHA pool, no-slip boundary conditions were specified with a wall roughness of 10 mm (for the full-scale model). For the lower plate, this roughness takes into account the presence of electrical heating and process gas injection for oxygen control. For the upper plate, it takes into account the presence of the grid, which prevents detached objects from floating into trapping spaces of the diaphragm. All other walls are considered as smooth walls with no-slip boundary conditions.

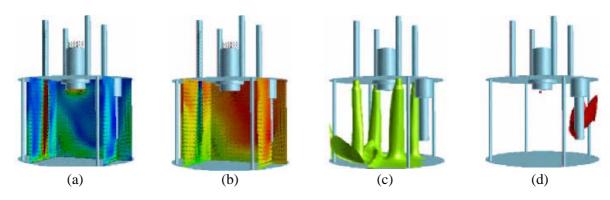
Results

Base Case and influence of stopped pumps

The flow field in the Base Case, with all pumps functioning, is shown in Figure 2. This figure also shows iso-surfaces of residence times. The residence time is the time the fluid needs to reach a certain point starting from the inlet. The flow field shows clearly the jets emerging from the pump outlets, reaching as far as the bottom plate.

Figure 2. Flow field [(a), (b)] and iso-surfaces [(c), (d)] of residence times for the Base Case

The contours in Figure 2(a) indicate the velocity. The contours in Figure 2(b) indicate the residence time. The residence time equals 170 s in Figure 2(c) and 270 s in Figure 2(d).



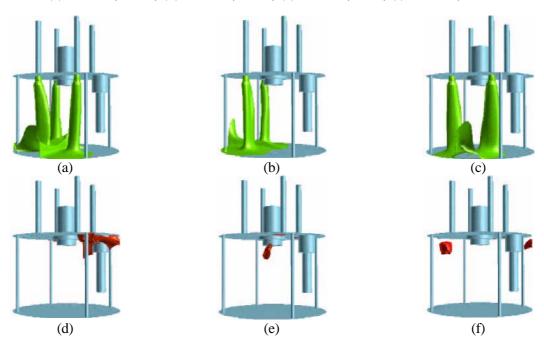
The maximum residence times of LBE in the MYRRHA pool as observed in the analyses are presented in Table 3. The maximum residence times increased with the number of stopped pumps. For the Base Case where all pumps are functioning, the maximum residence time was 280 s (as compared to the nominal value of 190 s, which is calculated by dividing the exchange volume of ~25 m³ by the throughput of all four pumps of 1 400 kg/s). For one stopped pump, the maximum residence time increased to approximately 430 s; whereas for two stopped pumps, the maximum residence time increased to ~600 s. This increase of residence time with the number of stopped pumps was caused by the decreased total mass flow rate since each stopped pump causes the total mass flow rate to decrease by 350 kg/s. The comparison of Cases 1a and 1b on one hand, and Cases 1c through 1f on the other hand, showed that the variation of the maximum residence time as a result of the mass flow rate distribution was ~15%. The occurrence of physico-chemical effects and precipitation had a typical timescale of several days. In comparison, the maximum residence times resulting from the analyses were lower by more than a factor of 100.

Table 3. Maximum residence times for the Base Case and Cases 1a through 1f

Case	Maximum residence time [s]
Base	280
1a	430
1b	360
1c	590
1d	560
1e	630
1f	600

Iso-surfaces of residence times are presented in Figure 3 for Cases 1a, 1c and 1e. Figures 3(a), 3(b) and 3(c) indicate which pumps are functioning and which are not functioning. Figures 3(d), 3(e) and 3(f) indicate the locations in the pool where the maximum residence times occur. Typically, the largest residence time occurs in the upper corners of the pool, where the side walls meet the upper grid and near the upper grid and target loop. The latter might change for the better if the spallation loop heat exchanger were modelled because that flow represents some 7% of the total throughput.

Figure 3. Iso-surfaces of residence times: (a) Case 1a, 250 s; (b) Case 1c, 370 s; (c) Case 1e, 370 s; (d) Case 1a, 380 s; (e) Case 1c, 580s; (f) Case 1e, 590 s



Different scaling methods

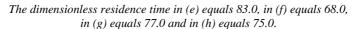
The maximum dimensionless residence times of lead-bismuth as observed in the MYRRHA pool are presented in Table 4. All dimensionless residence times were of the same order of magnitude. Where the characteristic time-based scaling (Case 2b) led to practically equal maximum residence times compared to the Base Case, the maximum residence time for the Reynolds number-based scaling (Case 2a) exceeded the maximum residence time of the Base Case by ~22% and the maximum residence time for the velocity-based scaling (Case 2c) exceeded the maximum residence time of the Base Case by ~7%. However, the occurrence of physico-chemical effects and precipitation had a typical timescale of several days. In comparison, even the residence times resulting from the Reynolds number-based scaling were lower by more than a factor 100.

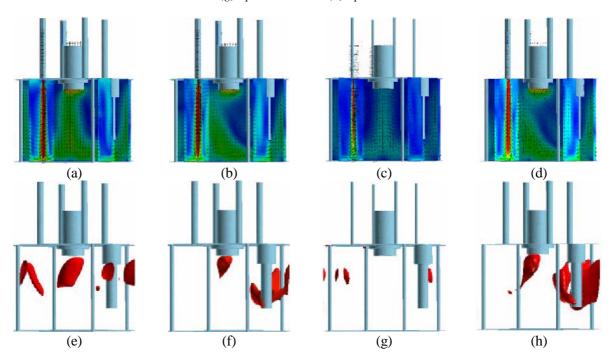
Table 4. Maximum dimensionless residence times for the Base Case and Cases 2a, 2b and 2c

Case	Maximum dimensionless
Case	residence time [-]
Base	73
2a	89
2b	72
2c	78

The contours of dimensionless velocity of the flow fields for Cases 2a, 2b and 2c are presented in Figure 4(a), 4(b) and 4(c). The flow fields of the Base Case and Case 2b were quite similar. The flow fields of the Base Case and Cases 2a en 2c were comparable, though less similar than the aforementioned. Iso-surfaces of dimensionless residence times are presented in Figure 4(e), 4(f) and 4(g). The residence time was chosen such that the figure indicates the locations of the largest residence times. The figure shows that the locations of maximum residence time are quite similar for the Base Case and Case 2b. Compared to this, there is less similarity between the locations of maximum residence times for the Base Case and Cases 2a en 2c.

Figure 4. Flow fields (dimensionless velocity) for Cases 2a (a), 2b (b), 2c (c) and 3 (d). Iso-surfaces of dimensionless residence times for Cases 2a (e), 2b (f), 2c (g) and 3 (h).





Different scaling factors

From the assessment of the different scaling methods, it was concluded that applying scaling based on characteristic time leads to a very similar flow topology compared to the Base Case. Therefore, the scaling is based on characteristic time (even for the analyses where different geometric scaling factors were applied).

The maximum dimensionless residence times of lead-bismuth in the lower MYRRHA pool as observed in the analyses are presented in Table 5. The maximum dimensionless residence times of the Base Case, Case 2b (scaling factor of five) and Case 3 (scaling factor of 10) are of the same order of magnitude. Both analyses of the scaled-down pool showed nearly equal maximum residence times compared to the Base Case. The maximum residence time of the scaled-down pool exceeded the maximum residence time of the full-scale pool with 11% maximum. Compared to the timescales of physico-chemical effects, both scaling factors resulted in a maximum residence time much lower than a factor of 100.

Table 5. Maximum dimensionless residence time for the Base Case and Cases 2b and 3

Case	Maximum dimensionless residence time [-]
Base	73
2b	72
3	81

The flow fields for Case 2b and Case 3 are presented in Figure 4(b) and 4(d). The analysed flow fields, with the scaling factor applied varying from zero to 10, were all very similar. Iso-surfaces of dimensionless residence times are presented in Figure 4(f) and 4(h). The figures show that the locations of maximum residence times were quite similar for scaling factors applied from zero to 10.

Conclusions and outlook

Based on the isothermal calculations performed in the lower part of the MYRRHA pool vessel, the following are concluded:

- The flow pattern behaves well, even in abnormal operational conditions with two pumps failing. The flow does not contain recirculation zones that result in large residence times or stagnant zones that could influence the cooling or physico-chemistry of the LBE.
- Applying a geometric scaling factor of five hardly changes the flow topology and the
 maximum residence times with respect to timescales for physico-chemical effects for all three
 considered scaling methods. Applying a geometric scaling factor of 10 marginally changes
 the flow topology and the maximum residence times. The scaling factor for a "small"-sized
 experiment of about eight can be seen as optimal from the point of view of flow similarity and
 volume reduction.

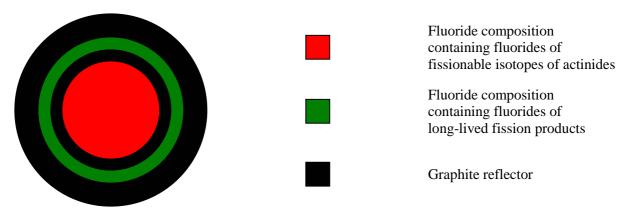
In the future, CFD analyses will be extended to cases where hot injection takes place and finally the full thermal cycle may be modelled.

REFERENCES

- [1] Aït Abderrahim, H., P. Kupschus, Ph. Benoit, E. Malambu, V. Sobolev, Th. Aoust, K. Van Tichelen, B. Arien, F. Vermeersch, D. De Bruyn, D. Maes, W. Haeck, "MYRRHA, A Multipurpose Accelerator Driven System for R&D. State-of-the-art Mid 2003", *Proceedings of the International Workshop on P&T and ADS Development*, SCK•CEN, BLG-959, ISBN 9076971072, Mol, Belgium (2003).
- [2] CFX5 User Guide, AEA Technology, Harwell, UK (1999).

- [3] Vieser, W., T. Esh, F. Menter, *Heat Transfer Predictions using Advanced Two-equation Turbulence Models*, CFX Validation Report CFX-VAL10/0602 (2002).
- [4] Kupschus, P, Vessel Layout c/w/ Spallation, E-mail sent on 11 April 2003.
- [5] Van Tichelen, K., Lead-bismuth Properties Database, SCK•CEN Report Number RF&M/KVT/kvt/32.B043000/85/01-47, Mol, Belgium (2001).

Figure 2. The schema of a transmuter elementary module with two primary circuits of molten fluorides



This concept is based on the idea of utilisation of efficient burning of transuranium nuclei in a large size fuel channel in the epithermal energy range where the majority of isotopes have resonances in their neutron cross-sections. It might be a critical system with reactivity and power controlled by specific flowing liquid fuel control systems (based on control of liquid fuel composition or its flow characteristics) or a subcritical system (with the subcriticality margin on the order of several betas) whose reactivity (keeping the prescribed level of subcriticality) is controlled in the same manner as in the above-described case of a critical system. Furthermore, the system is kept in a steady state and its power is controlled (driven) by an external neutron source or by a driving zone (part of a conventional reactor core).

The elementary module can be designed as a subcritical hexagonal fuel channel surrounded by six hexagonal graphite blocks, equipped with coaxial tubes (where molten fluorides of long-lived radionuclides may flow) that allow for efficient transmutation of long-lived radionuclides by an intensive flux of well-thermalised neutrons. These elementary modules represent an intensive source of energy and epithermal neutron flux that might be slowed down in graphite blocks and allow for very efficient incineration of at least some of the long-lived fission products in well-thermalised neutrons escaping the transmuter core. It should be noted that these elementary modules can be closely packed (joint) into a critical system or arranged in a complex of autonomous subcritical elementary modules that are driven by a set of external neutron sources or by a driving zone (a reactor core of another type surrounding the subcritical assembly of the molten fluoride elementary modules).

The two purposes of the proposed blanket system utilisation make usage possible as an efficient nuclear incinerator, actinide burner and, simultaneously, efficient energy source. Let us note that once such a system is developed and proven, it might serve as a new clean source of energy just by switching over from a uranium-plutonium fuel cycle to a thorium-uranium fuel cycle and thus excluding the generation of actinides. The main features of the SPHINX concept and the proof of individual processes as well as the corresponding technological and operational units of the nuclear "jeep" should be verified by the operation of a demonstration complex with power output on the order of 10 MWt. The concept of an experimental assembly of that type is introduced in Figure 3. Before we are able to design such a device, we must perform a broad experimental verification of design inputs for credible designing of a demonstration transmuter. The process of experimental verification recently (2002) began in the scope of the LA-10 project on the basis of preliminary preparation of an ideology of the experimental programme that was formulated earlier (in the scope of the LA-0 project in 1999 and 2000); some of its principle features were proven during this period. The experimental programmes and projects that have so far been developed/started will be described in the text that follows.

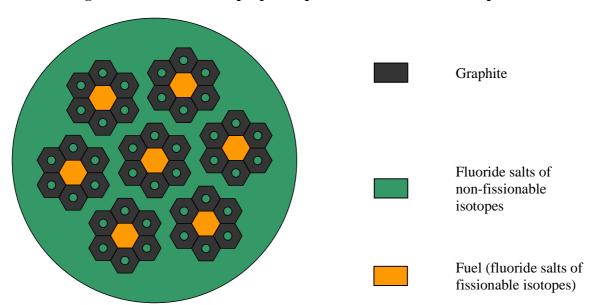


Figure 3. Subcritical dual-purpose experimental transmuter concept

Main experimental programmes started in the scope of the SPHINX project

The two specific features of the SPHINX project mentioned above, namely the chemical technology of the front end of the fuel cycle process and the neutronics (both static and kinetic) of the multi-purpose blanket with flowing liquid fuel, represent sufficiently new concepts to be calculated by modified computer codes that should be experimentally verified. Regarding the fluoride volatility process, we use as a base the knowledge gained from experience accumulated during the 1980s when we worked in close collaboration with the Russian Kurchatov Institute (RKI) in Moscow. During this time, such technology was developed and a pilot line was built and prepared for testing by processing hot spent fuel from the BOR60 fast reactor in the Atomic Reactor Research Institute (ARRI) in Dimitrovgrad. During the 1990s, this line was innovated and installed at NRI Rez and the first stage of testing for the SPHINX project was begun.

The new blanket concept was developed and proven by broad computer analyses in the second half of the 1990s. In the same time period, experimental programmes for verification of main neutronic characteristics including time behaviour were proposed. For this purpose, there are several large experimental devices operated in the scope of the Transmutation consortium. First of all, the experimental reactor LR-0 at NRI Rez and VR-1 at FNSPE are at our disposal as well as the NPI cyclotron accelerator that was equipped with a new target serving as an intensive neutron source. The VR-1 experimental reactor was equipped with the oscillator for the purpose of SPHINX-type blanket testing (namely, time behaviour and important safety characteristics). The first stage of experimental verification of some basic neutronic characteristics, reactor equipment and materials technology, and measurement techniques has already begun and involves experiments with inserted zones containing materials typical of our blanket concept and simulating neutronic features in a simplified model.

Technology of the new non-traditional materials in the SPHINX blanket is the subject of a broad R&D programme including experimental testing. For this purpose, a series of technological loops was erected by SKODA Nuclear Machinery plc, starting with laboratory equipment and continuing in a semi-pilot scale. The same is valid for the development of a technology for continuous cleaning up of circulating liquid fuel in the transmuter internal fuel cycle based on electro separation methods.

In 2000, the Technical University in Brno (TUB) was associated into the Transmutation consortium for the studying and testing of secondary cooling circuits of the LA-10 transmuter. The first step in an experimental programme in that field, the measuring bench, was erected and will serve for both measurement of basic technological characteristics of fluoride compositions and verification of design input for an auxiliary circuit of a molten fluoride media pantry in large loop testing complexes, which are being developed jointly by SKODA NM and Energovyzkum (EVM) Ltd. (a daughter company of TUB), as well as for the LA-10 demonstration transmuter.

The most important experimental program was started in 2001 and was based on experimental irradiation of blanket samples in the high neutron flux of research reactors. This programme is being carried out in close contracted collaboration with the RKI project AMPOULE and involves the development and validation of a modified reactor computer code based on a stochastic Monte Carlo model of neutron field long-term time behaviour in a system with circulating liquid fuel based on molten fluorides. The experimental irradiations are simultaneously performed at NRI and RKI in the first stage. The second stage representing irradiation of samples containing fluorides of actinides (Np, Pu, Am and Cm) was agreed to be performed and finalised jointly at RKI in 2002/2003. Some of the results of the preparatory (first) stage of this programme, which have already been obtained in NRI Rez in the scope of the BLANKA project, will be briefly introduced in the following section. We note that the proposal to start broad experimental verification of design inputs for a demonstration transmuter of the mentioned type was already put forth at the Fourth International ADTT&A'01 Conference in Reno, Nevada at the end of 2001 [3]. All of these experimental programmes were also (just recently) proposed to the Sixth Framework Programme of the European Commission.

The programme of irradiated probes and BLANKA instrumented rigs

The very first idea for this programme was initiated by RKI as early as the late 1980s when some very preparatory irradiations and measurements were performed in the Tashkent research reactor. On the basis of the obtained experience, the project AMPOULE was developed at RKI in the 1990s. After a period of pre-contract negotiations in the second half of the 1990s, the bilateral contract was finally agreed upon and signed in July 2001. Immediately thereafter the first stage of the joint development of the modified reactor computer code ISTAR (based on a stochastic Monte Carlo model of neutron field long-term time behaviour in a system with circulating liquid fuel based on molten fluorides) started in autumn 2001. At the same time, preliminary irradiations, measurements and evaluations were performed on the LVR-15 research reactor at NRI with the aim to be able to design and perform the regular programme of irradiated BLANKA probes, serving as validation of the developed computer code.

During the same time frame, an elementary metallic probe and a complex of irradiated probes were performed, which lead to the realisation of BLANKA instrumented rigs. The first series, BLANKA 100 (identical in size to one fuel assembly of both the VR-1 experimental and LVR-15 research reactor), was designed and tested at NRI during 2001. Preliminary tests of the rig neutronic characteristics started in December 2001 on the experimental reactor VR-1 at the Czech Technical University in Prague. Then, a series of first irradiations were performed on the NRI research reactor LVR-15 in January and February 2002. The series of irradiation tests called BLANKA 101 were curried out with empty probes (no fluoride content), serving just for the tuning of all measuring channels and verification of design-predicted characteristics (temperature and pressure fields in particular).

After an evaluation of the obtained results, the first experiments were performed in April 2002 using probes containing pure NaF and/or NaF with an admixture of metallic Mo powder, modelling the presence of fission product. The probe, BLANKA 102, was inserted in the core of the research reactor at its very edge with a low value of neutron flux where heating of the probe is generated nearly

by gamma capture only. The temperature field was measured by a set of five independent thermocouples located in different positions in the elementary probe room. Figure 4 shows the results of a continuous measurement of gas pressures in individual layers of the BLANKA 102 probe during irradiation. The decrease of the pressure of the noble gas (Ar) filling the elementary probe at 11:30 on April 17 is caused by the testing of a controlled discharge of expected gaseous fission products in the case of the fluoride composition containing components of fluorides of fissionable metals.

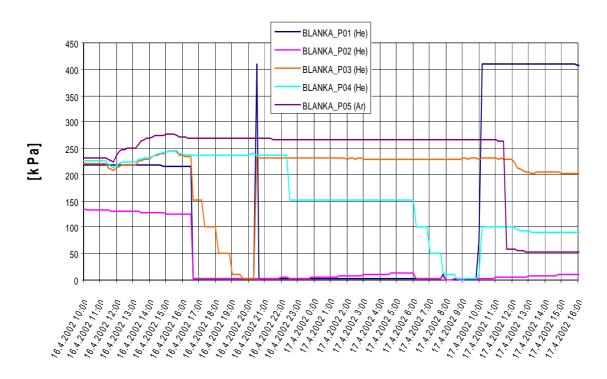


Figure 4. Results of measurements of gas pressures in individual layers of BLANKA 102 probe

After evaluation of BLANKA 101 and 102 test results, some convenient small rearrangements were applied in the prepared new version of the BLANKA 103 probe, which were used in the experimental programme performed during the first half of 2003. The majority of the irradiated samples were based on a composition of $^{7}\text{LiF} + \text{NaF}$. The admixture of modelling fission products and finally even an admixture of a small amount of UF₄ were incorporated into the individual sample compositions. An exact description of the BLANKA 103 sample content can be seen in Figure 5.

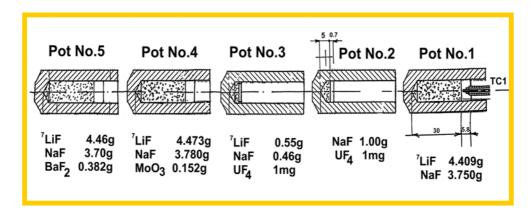


Figure 5. Contents of the BLANKA 103 sample pots

fluorides

graphite

air

Fe reflector

meas.
channels
channels

Figure 6. The simplified model of the BLANKA 400 rig for neutronic tests at room temperature

Following the experience accumulated during the BLANKA 100 instrumented rigs, the larger size series (identical to the area of four fuel assemblies) called BLANKA 400 was designed and preliminary tests started on the VR-1 experimental reactor at the end of 2003 under room temperature and low level of neutron flux conditions. For these neutronic tests, the simplified version manufactured from nuclear aluminium structural material (see Figure 6) was used. Once again, the first series of experiments was performed with pure NaF in tubes A, B and C, starting at the beginning of 2004 and due to finish by 31 May 2004. The same model was to serve for an adjustment of the testing facility with the external neutron source NG1 on external beam line of the isochronous cyclotron U-120M at NPI during the second half of 2004. During this time, neutronic experiments with BLANKA 400 filled in by LiF + NaF compositions in various ratios were forecast to take place at the VR-1 experimental reactor.

Conclusions

Principle features of the SPHINX project involving the development of a transmuter with liquid fuel based on molten fluorides and a connected R&D programme were described in necessary detail. The experimental part of the R&D programme of the SPHINX project was briefly introduced, which serves as verification of design inputs for designing a demonstration unit of a transmuter with liquid fuel based on molten fluorides. Due to the current status of the experimental programme, performance was focused on the irradiation of samples of molten salt systems as well as structural materials proposed for the blanket of the SPHINX transmuter in the field of high neutron flux of research reactors (attention focused on the latter part). We should underline that the main aims of this programme (called BLANKA irradiated probes) are the following:

• Experimental verification of long-time behaviour of transmuter blanket, which contains molten fluoride salts as fuel and graphite as moderator or reflector.

Material research on behaviour of materials in neutron and gamma fields, and material
interactions in high temperature conditions. Validation of computational codes (system of
codes NJOY – preparation of data library for MCNP; MCNP – computation of cross-sections
for the code ISTAR being developed for the computation of actinide concentration in
long-term operation of the transmuter).

Preliminary experiments have been performed by irradiation of simplified samples of fluorides of non-fissionable metals since mid-2001. The first experiment with the instrumented rig BLANKA 101, which served for the tuning of measuring methods and channels, started in December 2001. In this experiment, the probe without fluorides was inserted into the core of the LVR-15 research reactor in NRI Rez for a few days of irradiation on different levels of the reactor power (neutron flux). The second BLANKA 102 experiment was conducted in April 2002 when two samples were irradiated – one containing pure NaF and another containing NaF with an admixture of Mo metallic powder (modelling a fission product). Measurements and experience collected in this stage fully confirmed the principle correctness of design and operational properties of the programme of BLANKA instrumented rigs, serving as irradiation tests of transmuter blanket material samples under conditions close to operational.

After the evaluation of BLANKA 101 and 102 test results, some convenient small rearrangements were applied in the prepared new version of the probe BLANKA 103 and they were used in the experimental programme performed during the first half of 2003. Nearly all of the irradiated samples were based on a composition of ⁷Li + NaF. The admixture of modelling fission products and finally even an admixture of a small amount of UF₄ were incorporated into individual sample compositions. There was also the insertion of structural material samples (also a subject of broad non-active and pre-irradiation technological testing), which were supposed to be irradiated and preliminarily tested in these irradiations. At the same time, the preliminary neutronic tests of the larger sized version (equal to the area of four quadratic fuel assemblies of VR-1 or LVR-15 reactor) of the BLANKA 400 rig started using a simplified aluminium model at room temperature inserted into the VR-1 experimental reactor and into the testing facility with the external neutron source NG1 on the external beam line of the isochronous cyclotron U-120M in NPI. We will be able to report later this year on results obtained in these experimental programmes.

Acknowledgements

The SPHINX project was proposed at the end of 1996 by the Transmutation consortium established by four leading nuclear research bodies in the Czech Republic (Nuclear Research Institute Rez plc, SKODA Nuclear Machinery plc in Pilsen, the Nuclear Physics Institute of Academy of Sciences in Rez and the Technical University in Prague) to whom Technical University in Brno (specialised in secondary circuit problems) associated in 2000. The project has been supported by the Ministry of Industry and Trade of the Czech Republic, CEZ a.s. (Czech Power Company) and RAWRA (Radwaste Repository Authority). At present, two agreements on multi-national co-operation in this field have been signed – one with the European Commission (project MOST) and one with the Russian Kurchatov Institute. The experimental programme of project SPHINX was proposed to the Sixth Framework Programme of the European Commission for the period 2004-2008.

The authors would like to acknowledge all the support the project has received so far and to express their hope that understanding will continue as progress is made towards the efficient resolution of crucial issues on nuclear power and as successful development takes place in this new era.

REFERENCES

- [1] Hron, M., "A Preliminary Design Concept of the Experimental Assembly LA-0 for Accelerator-driven Transmuter Reactor/Blanket Core Neutronics and Connected Technology Testing", Report LA-UR 95-3761, Los Alamos National Laboratory, New Mexico, USA (1995).
- [2] Hron, M., "National R&D Program of Nuclear Incineration of PWR Spent Fuel in a Transmuter with Liquid Fuel as Being Developed in the Czech Republic", ADTT&A'99, Prague-Pruhonice, Czech Republic, 7-11 June 1999.
- [3] Hron, M., "Experimental Verification of Selected Transmutation Technology for a Design Development of Basic Components of the Demonstration Transmuter LA-10 (Development of New Technologies for Nuclear Incineration of PWR Spent Fuel in the Czech Republic)", Fourth International Conference ADTT&A'01, Reno, Nevada, November 2001.
- [4] Hron, M., *et al.*, "Project SPHINX Spent Hot Fuel Incineration by Neutron Flux (Experimental Verification of Design Inputs for Transmuter with Liquid Fuel Based on Molten Fluorides)", 11th International Conference on Emerging Nuclear Energy Systems, Albuquerque, New Mexico, 29 September 4 October 2002.

APPLICATION OF THE HYPER SYSTEM TO THE DUPIC FUEL CYCLE

Yonghee Kim, Tae-Yung Song

Korea Atomic Energy Research Institute 150 Duckjin-Dong, Yuseong, Daejeon 305-353, Korea

Abstract

This paper is concerned with the transmutation of TRUs in DUPIC (direct use of spent PWR fuel in CANDU) spent fuel in the HYPER system, which is an LBE-cooled ADS. The DUPIC concept is a synergistic combination of PWR and CANDU, in which PWR spent fuels are directly re-utilised in CANDU reactors after a very simple refabrication process. The objective of this study is to investigate the TRU transmutation potential of the HYPER core for the DUPIC-HYPER fuel cycle. All the previously developed HYPER core design concepts were retained except those which involve fuel composed of TRUs from DUPIC spent fuel. The HYPER core characteristics were analysed using the REBUS-3/DIF3D code system.

Introduction

A lead-bismuth eutectic (LBE) cooled 1 000 MWth ADS, which is called HYPER [1,2] (hybrid power extraction reactor), is being studied in Korea for the transmutation of TRUs and LLFPs. This paper is concerned with neutronic design characteristics of the HYPER core and its transmutation capability. Previously, the HYPER system was devoted to the transmutation of TRUs and LLFPs from PWR spent fuels, where the PWR spent fuel was reprocessed with simple pyro-processing and the recovered TRUs were incinerated in the HYPER core [2]. In this paper, a different transmutation fuel cycle is studied in order to ameliorate the spent fuel issue in Korea.

Korea is the only country that has both commercial PWRs and CANDUs in operation. Currently, there are 14 PWRs and four CANDUs in Korea. Currently, the CANDU reactor utilises natural uranium and, consequently, the fuel discharge burn-up is fairly low (~7 500 MWD/MTU), producing much more spent fuel compared to PWRs. In order to mitigate the CANDU spent fuel issue and to improve uranium utilisation, a tandem fuel cycle is being studied/developed in Korea. The fuel cycle is called DUPIC (direct use of spent PWR fuel in CANDU) [3] and is indigenous to Korea. In the DUPIC fuel cycle, the PWR spent fuel is reused in CANDU after a very simple refabrication process, which consists only of oxidation, and reduction (OREOX) processes and sintering. In the dry OREOX processing, even fission gases are not fully removed from the spent fuel. Thus, the DUPIC cycle is considered to be extremely proliferation-resistant. For a 35 GWD/MTU PWR spent fuel, a DUPIC fuel can be reused up to 15 GWD/MTU in the CANDU core. Therefore, ~22% uranium savings is possible and the spent fuel production is reduced by ~67%. The DUPIC study shows that the DUPIC fuel cycle cost is comparable to conventional once-through fuel cycles.

In the DUPIC-HYPER fuel cycle, TRUs from DUPIC spent fuel are transmuted in the HYPER core. Basically, the fuel cycle for HYPER is the same as in the previous PWR-HYPER case. The objective of this study is to investigate the TRU transmutation potential of the HYPER core for the DUPCI-HYPER fuel cycle. All the previous HYPER design concepts are applied to the new core design except that the fuel is composed of DUPIC TRUs. The core characteristics of HYPER are analysed with the REBUS-3/DIF3D code system.

The major mission of the HYPER system is to transmute as much as possible the TRUs in such a way that the associated fuel cycle is as proliferation-resistant as possible. For a proliferation-resistant fuel cycle, the so-called pyro-processing of spent fuels is utilised in HYPER. In the front-end reprocessing of DUPIC spent fuel, the uranium and rare earth (RE) element removal rates were 99.9% and 99%, respectively. On the other hand, only fission products are removed from HYPER spent fuel, where 95% of REs are assumed to be removed without any separation of TRUs as in the previous PWR-HYPER case.

Design features of the HYPER core

Figure 1 shows a schematic configuration of the HYPER core with 186 ductless hexagonal fuel assemblies. As shown in Figure 1, the fuel blanket is divided into three TRU enrichment zones to flatten the radial power distribution. In HYPER, a beam of 1 GeV protons is delivered to the central region of the core to generate spallation neutrons. To simplify the core design, the LBE coolant is also used as a spallation target. In addition to the ultimate shutdown system (USS), six safety assemblies are placed in the HYPER core for use in an emergency. The safety rods are used conditionally to control the reactivity of the core. For a balanced transmutation of TRUs and LLFPs, ⁹⁹Tc and ¹²⁹I are incinerated in moderated LLFP assemblies loaded in the reflector zone.

A preliminary study on the optimal range of subcriticality showed that subcriticality of the HYPER core might be in the range $0.961 < k_{\rm eff} < 0.991$, subject to the constraint of 20 MW maximum accelerator power [4]. (This is considered as the maximum allowable beam power for the target window design of the HYPER system). The maximum allowable $k_{\rm eff}$ of the HYPER core was set to 0.98 during a normal operation through an iterative analysis of system safety and its technical feasibility. In the HYPER target design, we introduced an LBE injection tube to maximise the allowable proton beam current. The injection tube controls the LBE flow rate in the target channel such that the central flow rate is higher than that in the peripheral zone. With the aid of the injection tube, the beam window can be very efficiently cooled and the LBE flow rate in the target channel can be substantially reduced, thereby reducing the coolant pumping power. It is important to note that the reduced LBE flow rate in the target channel increases the temperature of the target LBE. Preliminary analysis for a dual injection tube showed that a 20 MW beam power could be accommodated with a sufficient margin for a flat beam profile [5].

It is well known that the LBE coolant speed is limited (usually < 2 m/sec) due to its erosive and corrosive behaviour. Therefore, the lattice structure of the fuel rods should be fairly sparse. In fast reactors, a pancake-type core is typically preferred mainly to reduce coolant pressure drop. Unfortunately, it has been found that the multiplication of the external source is quite inefficient in a pancake-type ADS because of the relatively large source neutron leakage. Kim, *et al.* [6], have shown that the maximum source multiplication can be achieved when the core height is ~2 m. Taking into account the source multiplication and the coolant speed, the core height of HYPER was compromised at 150 cm, and the power density was determined such that the average coolant speed could be ~1.65 m/sec. The inlet and exit coolant temperatures in the core are 340°C and 490°C, respectively. To reduce core size and to improve neutron economy, a ductless fuel assembly is adopted in the HYPER system. An advantage of ductless fuel assembly is that the flow blockage of a subassembly is basically impossible and the production of activation products in the duct is avoidable.

In general, a non-uranium alloy fuel is utilised in a TRU transmuter to maximise the TRU consumption rate. Previously, a Zr-based dispersion fuel was used as the HYPER fuel since it was expected that a very high fuel burn-up could be achieved. However, we found that the dispersion fuel transforms to a metallic alloy during high temperature operation. Therefore, in the current design the metallic alloy of U-TRU-Zr is used as the HYPER fuel (where pure lead is the bonding material). As a result, a large gas plenum is placed above the active core.

Concerning a TRU-loaded ADS, which uses a fixed cycle length, one of the challenging problems is a very large reactivity swing, leading to a large change in the accelerator power over a depletion period. Even in an ADS loaded with MA (minor actinide) fuel, the burn-up reactivity swing is found to be fairly noticeable, although it is relatively smaller than that in a TRU-loaded core. The large burn-up reactivity swing results in several unfavourable safety features as well as deleterious impacts on the economics of the system. In the HYPER core, ¹⁰B was used as a burnable absorber (BA) in a unique way so as to reduce the reactivity swing and to control the core power distribution [2].

Each fuel assembly has 204 fuel rods and the fuel rods are aligned in a triangular pattern with 13 tie rods. A fairly open lattice with a pitch-to-diameter (P/D) ratio of 1.49 is adopted in HYPER. Table 1 shows the major design parameters of the HYPER fuel assembly. In Figure 2, a schematic configuration of the ductless fuel assembly is shown. The ¹⁰B burnable absorber is loaded into the tie rods with top and bottom cutbacks in order to enhance the ¹⁰B depletion rate and also to flatten the axial power distribution of the core. The BA concept with the cutbacks can effectively mitigate the peak fast neutron fluence of the assembly. The peak fast neutron fluence is a limiting design criterion in LBE-cooled fast reactors.

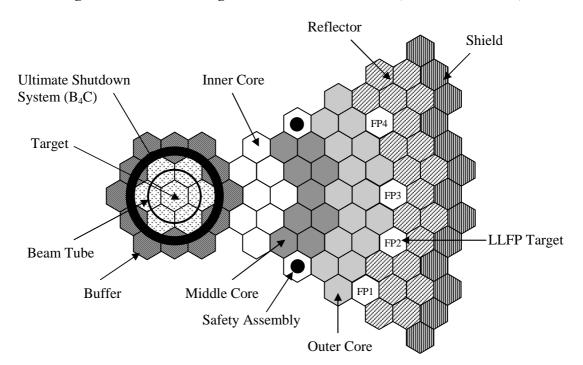


Figure 1. Schematic configuration of the HYPER core (186 fuel assemblies)

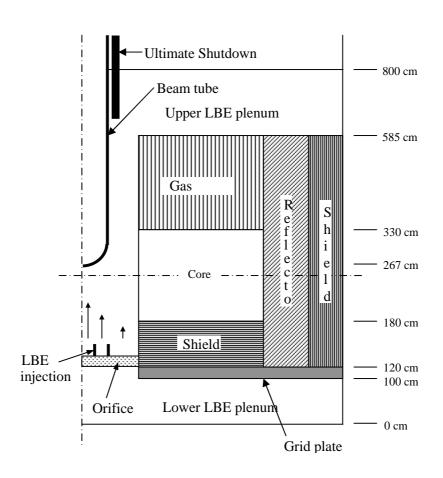
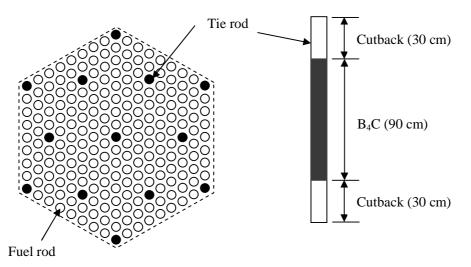


Table 1. Ductless fuel assembly design

Fuel material	Metallic alloy: U-TRU-Zr
Cladding and tie rod material	HT-9
Number of fuel pins per assembly	204
Number of tie rods	13
Pin diameter (cm)	0.77
Cladding thickness (cm)	0.060
Pitch/diameter ratio	1.49
Fuel smear density (% T.D.)	75
Outer radius of tie rod (cm)	0.44
Inner radius of tie rod (cm)	0.36
Active length (cm)	150
Interassembly gap [fuel-to-fuel] (cm)	0.34
Assembly pitch (cm)	17.0075

Figure 2. Configuration of the ductless fuel assembly with B₄C burnable absorber



Neutronic performance of the HYPER core

In this section, we discuss the neutronic analysis of the HYPER core, which was performed with the REBUS-3 [7] code system. The core depletion analysis was based on the equilibrium cycle method of REBUS-3. The flux calculations were performed over a nine-group structure with hexagonal-Z models using a nodal diffusion theory option of the DIF3D code [8]. The region-dependent, nine-group cross-sections were generated using the TWODANT [9]/TRANSX [10] code system based on the data of ENDF/B-VI. For the external source in a central target zone, a pre-calculated generic source distribution was used.

In the REBUS-3 depletion analysis, it was assumed that 99.9% of the discharged fuel elements are recovered and recycled into the core after a one-year cooling time. In this work, 5% of the rare earth elements are carried over during the fuel reprocessing/fabrication processing since it is difficult to completely separate them from the fuel material.

Regarding fuel management, a scattered fuel assembly reloading is used as in conventional fast reactors since a whole-core fuel shuffling might be time-consuming in an LBE-cooled reactor and its effects would not be significant. A relatively short cycle length (half-year cycle with 146 EFPDs) is adopted in HYPER to reduce the burn-up reactivity swing. As a result, the batch size should be large to achieve a high fuel burn-up. For the inner zone, seven-batch fuel management is applied and an eight-batch scheme is applied to middle and outer zones. Consequently, the number of fuel assemblies to be reloaded in a cycle in each zone is six (inner), six (middle) and 12 (outer). In the actual scattered fuel reloading, the fuel enrichment of each fuel assembly in each zone needs to be adjusted to obtain the required subcriticality and acceptable power distribution. Thus, it is assumed that fuel enrichment is different depending on the fuel assemblies in each zone – the number of fuel enrichment splittings is four (inner core), five (middle core) and five (outer core). It is worthwhile to note that four types of fuel assemblies are needed for every reload cycle due to fuel management schemes.

In addition to the half-year cycle length, both the ¹⁰B burnable absorber and control rods are used to further reduce the reactivity swing in the HYPER core. In the case of ¹⁰B burnable absorber usage, B₄C is only loaded into the relatively high-flux zones to enhance burn-up rate since the burn-up penalty would be too serious if discharge burn-up were too low (see Figure 2). Also, it is important to note that BA is not applied to the inner core because an absorber near the external source significantly reduces the degree of source multiplication, hence increasing the required accelerator current. In the current design, natural enriched B₄C is used in the middle and outer cores. With the above fuel management schemes, the REBUS-3 analyses were performed for three different core designs in order to assess the effects of the burnable absorber and control rods on the core performance. The numerical results are summarised in Table 2 in terms of several important core parameters.

In Table 4, it is observed that burn-up reactivity swing in the ¹⁰B-loaded core was reduced by ~33%, relative to the reference BA-free core design. However, fuel inventory is also increased by ~21% in the BA-loaded core due to the relatively slow depletion rate of the ¹⁰B BA. The discharge burn-up of ¹⁰B is ~55%. The increased fuel inventory in the BA-loaded core resulted in a reduced fuel discharge burn-up (from 21.2% to 17.9%). It is worthwhile to note that the power peaking factor is a little smaller in the BA-loaded core. This is because the ¹⁰B BA was loaded with the top and bottom cutback zones, i.e. the axial power distribution is more flattened in the BA-loaded core. Consequently, the peak fast neutron fluence is significantly smaller in the BA-loaded core. The net fuel consumption rate is virtually independent of the BA loading, thus, the two cores have an almost identical TRU transmutation rate, 272 kg/year. However, the fuel mass, which should be reprocessed and refabricated, is larger in the BA-loaded core due to the increased fuel inventory.

Table 2 shows that the maximum proton current is still larger than 20 mA even in the BA-loaded core. Meanwhile, it is clear that the proton current is smaller than 20 mA when both BA and control rods are simultaneously utilised without compromising fuel discharge burn-up. This is because the inserted control rods are all fully withdrawn in the middle of the cycle. It is worthwhile to note that the $k_{\rm eff}$ value is still smaller than 0.99 when all the control rods are withdrawn at BOC, satisfying the subcriticality requirement of the HYPER core.

From Table 2 one can note that the source importance in HYPER cores is fairly high. High source importance is mainly attributed to the relatively high H/D ratio of the HYPER core. It is observed that source importance at EOC is just slightly lower than at BOC due to the accumulation of fission products. The BA-loaded cores have a slightly smaller source importance because of the presence of ¹⁰B absorber.

It is observed that ¹⁰B BA slightly reduces delayed neutron fraction and makes neutron generation time noticeably shorter. Table 2 also compares the coolant void reactivity of the three cores. In the void reactivity evaluation, it was assumed that all the coolant was voided only in the active core. It is clear that the BA-loaded cores have a much larger void reactivity. This is because the capture cross-section of the ¹⁰B isotope decreases as the neutron spectrum becomes harder. We think that positive void reactivity would be acceptable since active-core-only voiding is basically impossible in an LBE-cooled reactor.

Table 2. Equilibrium cycle performance of the HYPER cores

Parameter		Without BA and CR	With BA only	With BA and CR
	Inner zone	37.0	41.5	42.7
Average fuel weight fraction (%)	Middle zone	41.7	46.6	47.3
	Outer zone	45.5	51.7	52.2
Effective full-power day [EFPD] (c	lays)	146	146	146
Effective multiplication factor	BOC	0.9801	0.9801	0.9804 (0.9898*)
(k _{eff})	EOC	0.9504	0.9603	0.9701
Source importance (BOC/EOC)		(0.90/0.89)	(0.87/0.85)	(0.88/0.87)
Burn-up reactivity loss (% Δk)		2.97	1.98	1.03
Proton current [BOC/EOC] (mA)		(11.3/29.0)	(11.7/24.1)	(11.4/17.7)
β_{eff} , neutron generation time	BOC	0.00288, 2.06	0.00280, 1.65	0.00279, 1.52
(µsec)	EOC	0.00291, 2.21	0.00283, 1.76	0.00282, 1.68
Core average power density (kW/l)		143	143	143
3-D power peaking factor (BOC/E0	OC)	(1.60/1.77)	(1.52/1.71)	(1.54/1.60)
Linear power [average, peak] (kW/	m)	(17.6, 31.2)	(17.6, 30.1)	(17.6, 28.2)
Average fuel discharge burn-up (a/	0)	21.2	17.9	17.5
BOC ¹⁰ B inventory (kg)		-	13.9	13.9
Peak fast fluence (n/cm ²)		3.8×10^{23}	3.2×10^{23}	3.2×10^{23}
Fuel consumption [U/TRU] (kg/year)		(32/272)	(32/272)	(32/272)
Heavy motel inventory (kg)	BOC	5 007	6 075	6 210
Heavy metal inventory (kg)	EOC	4 855	5 923	6 058
Active core void reactivity [BOC/E	Active core void reactivity [BOC/EOC] (pcm)			(1 749/1 875)

 $[*]k_{eff}$ in all-rod-out condition

In Figure 3, assembly power distributions are provided for both BOC and EOC of an equilibrium cycle for the three HYPER cores. One can see that the inner zone power increased while the outer zone power decreased as the core burn-up increased. This behaviour is generally observed in a TRU-loaded ADS core and is due to the reactivity loss of the core with burn-up. It is noteworthy that the change in the spatial power distribution is significantly mitigated in the core with the control rods, which is ascribed to the smaller reactivity swing in the core. Instead of using control rods, the maximum proton current could be reduced below 20 mA by simply increasing $k_{\rm eff}$ up to 0.99 at BOC. However, in this case, substantial slanting behaviour in the power distribution still occurs since the reactivity swing is fairly large. This is one of the motivations for using the control rods to compensate for reactivity change in HYPER.

Table 3 compares the fuel composition vectors at three fuel management stages (feed, charge and discharge) for an equilibrium cycle of the BA-loaded core with control rods. It is clearly seen that ²⁴⁰Pu has the largest weight per cent in the equilibrium cycle while ²³⁹Pu is the most dominant isotope in the feed fuel composition. One can find the ²³⁹Pu fraction in the feed fuel relatively small compared with typical PWR spent fuel, where ²³⁹Pu weight fraction is usually ~50%. This is because ²³⁹Pu is burned most efficiently in the CANDU core. It is noteworthy that weight fractions of the higher actinides such as Am and Cm are significantly increased in the equilibrium core. Also, it is important to note that the weight fraction of the ²³⁸U isotope almost doubled in the equilibrium core compared with the feed fuel. The RE fraction in the charging fuel is relatively noticeable.

0.98 1.05 0.94 1.01 0.98 1.05 1.06 1.01 0.89 1.05 1.06 0.91 0.98 1.06 1.04 0.97 1.04 1.07 0.99 1.00 0.94 1.051.06 1.06 0.98 1.06 1.07 1.02 1.06 1.04 1.07 1.04 0.97 0.94 0.98 1.03 1.05 1.01 0.89 0.98 1.05 1.01 0.94 0.99 0.95 No BA and 0.980.99 0.97 0.96 0.97 1.00 0.98 1 04 0.96 1.01 0.95 1.01 1.00 1.01 1.03 1.02 1.04 1.03 0.99 1.05 1.02 1.02 1.01 1.03 1.01 0.91 1.06 1.02 1.03 1.01 0.99 1.05 1.05 1.03 1.02 1.03 1.05 1.03 1.00 1.05 1.04 BOC 0.99 1.04 1.05 1.02 1.03 0.95 1.05 1.02 1.05 1.01 1.03 0.98 1.03 1.03 1.03 1.04 EOC 1.05 1.03 1.02 1.01 1.03 1.05 0.99 1.05 0,88 1.04 1.03 1.03 1.05 1.03 1.00 1 04 1.03 0.95 1.04 1.00 1.01 0.95 1.03 1.01 0.92 1.01 0.91 1.00 0.97 1.04 0.98 1.01 0.96 0.95 1.01 0.98 0.99 0.96 With BA and CR With BA only

Figure 3. Relative assembly power distributions in HYPER cores

Table 3. Fuel composition in an equilibrium cycle core with BA and CR

Isotope	Feed	Charge	Discharge
²³⁴ U	2.47E-3	0.53	0.48
²³⁵ U	0.032	0.14	0.13
²³⁶ U	0.049	0.28	0.26
²³⁸ U	10.01	19.59	17.85
²³⁷ Np	4.55	2.07	1.27
²³⁸ Pu	3.53	4.43	3.69
²³⁹ Pu	33.72	15.82	9.86
²⁴⁰ Pu	27.28	28.95	23.96
²⁴¹ Pu	3.06	4.07	3.82
²⁴² Pu	8.66	11.46	9.92
²⁴¹ Am	6.23	4.30	2.91
²⁴² Am	0.0072	0.24	0.24
²⁴³ Am	1.32	3.52	3.29
²⁴² Cm	1.73E-5	0.016	0.20
²⁴³ Cm	0.020	0.024	0.021
²⁴⁴ Cm	0.21	2.69	2.83
²⁴⁵ Cm	0.0050	0.87	0.87
²⁴⁶ Cm	0.0033	0.58	0.58
RE	1.33	0.41	3.56
FP*	0.0	0.0	14.27

*without RE

Conclusions

A DUPIC-HYPER fuel cycle was studied to transmute TRUs contained in DUPIC spent fuel. It was found that fuel inventory is slightly larger in the DUPIC-HYPER fuel cycle due to a degraded plutonium vector than in the previous PWR-HYPER cycle. Consequently, burn-up reactivity swing is calculated to be a little smaller in the DUPIC-HYEPR case. However, without any design measure to reduce reactivity swing, the required maximum proton current was 29 mA, which is far beyond the targeted value of 20 mA. The reactivity swing was reduced by \sim 33% by introducing a B₄C burnable absorber with top/bottom cutbacks. Furthermore, conditional utilisation of control rods (CR) together with B₄C BA results in a maximum proton current of \sim 18 mA. It was confirmed that B₄C BA could substantially reduce fast fluence.

For a reference HYPER core without BA and CR, the core consumes ~272 kg of TRU per year with a fuel discharge burn-up of ~21 a/o. In the BA-loaded BA and CR cores, the TRU consumption rate is basically the same, but the fuel discharge burn-up is ~18 a/o due to the residual reactivity penalty of the B_4C BA. Also, it was found that control rods can be effectively utilised to mitigate the slanting behaviour of the radial power distribution in the HYPER core.

REFERENCES

- [1] Park, W.S., *et al.*, "HYPER (Hybrid Power Extraction Reactor): A System for Clean Nuclear Energy", *Nuclear Engineering and Design*, 199, p. 155 (2000).
- [2] Kim, Y., *et al.*, "Core Design Characteristics of the HYPER System", OECD/NEA 7th Information Exchange Meeting on Actinide and Fission Product Partitioning & Transmutation, Jeju, Korea, 14-16 October 2002.
- [3] Ko, W.I., *et al.*, "Economic Analysis on Direct Use of Spent Pressurized Water Reactor Fuel in CANDU Reactors IV: DUPIC Fuel Cycle Cost", *Nuclear Technology*, 134, 167 (2000).
- [4] Kim, Y., et al., "An Investigation of Subcriticality Level in Accelerator-driven System", Proceedings of the PHYSOR 2002 International Conference on the New Frontiers of Nuclear Technology, Seoul, Korea, 7-10 October 2002.
- [5] Cho, C.H., *et al.*, "The Introduction of a Double-annular Guide Tube for the Design of 20 MW Lead-bismuth Target System", OECD/NEA Fourth International Workshop on Utilization and Reliability of High Power Proton Accelerators, Daejeon, Korea, 16-19 May 2004.
- [6] Kim, Y., *et al.*, "Optimization of Height-to-diameter Ratio for an Accelerator-driven System", *Nuclear Science and Engineering*, 143, 141 (2002).
- [7] Toppel, B.J., "A User's Guide to the REBUS-3 Fuel Cycle Analysis Capability", ANL-83-2, Argonne National Laboratory (1983).
- [8] Derstine, K.L., "DIF3D: A Code to Solve One, Two, and Three-dimensional Finite Difference Diffusion Theory Problems", ANL-82-64, Argonne National Laboratory, April 1984.
- [9] Alcouffe, R.E., *et al.*, "User's Guide for TWODANT: A Code Package for Two-dimensional, Diffusion-accelerated Neutral Particle Transport", LA-10049-M, Los Alamos National Laboratory (1990).
- [10] MacFralane, R.E., "TRANSX2: A Code for Interfacing MATXS Cross Section Libraries to Nuclear Transport Codes", LA-12312-MS, Los Alamos National Laboratory (1992).

NUMERICAL COMPARISONS BETWEEN NEUTRONIC CHARACTERISTICS OF MUSE4 CONFIGURATIONS AND XADS-TYPE MODELS

M. Plaschy¹, S. Pelloni¹, P. Coddington¹, R. Chawla^{1,2}, G. Rimpault³, F. Mellier³
¹Paul Scherrer Institute, Villigen (PSI), Switzerland; michael.plaschy@psi.ch
²Swiss Federal Institute of Technology (EPFL), Lausanne, Switzerland
³DEN/DER, CEA/Cadarache, Saint-Paul-lez-Durance, France

Abstract

The representativity of a specific MUSE4 configuration (M4SC2) was analysed from a nuclear data viewpoint, with respect to the current concepts of experimental accelerator-driven systems (XADSs) with gas (He), Na and Pb/Bi coolants. In this context, data sensitivity/uncertainty analyses based on first order perturbation theory calculations were performed using the deterministic code ERANOS (Version 2.0) in conjunction with its adjusted nuclear data library ERALIB-1, which lead to the determination of suitable representativity factors.

It was found that M4SC2 is quite representative of XADS with He and Na. However, in the case of a Pb/Bi system, the effects of significant uncertainties associated with the data for these two nuclides and their low content in M4SC2 were clearly highlighted, resulting in much lower representativity factors. Thus, the need for additional experiments was evident.

Introduction

In the field of waste management incorporating a transmutation option, accelerator-driven systems (ADS) represent an important alternative to conventional reactors due to their higher safety level when minor actinides such as Np and Am are loaded into the core. As a result, it is necessary to extend the validation domain of calculation methods for critical fast reactors to the analysis of source-driven subcritical configurations.

To reach this goal, the experimental program MUSE was launched in the MASURCA facility at CEA/Cadarache (France). Of particular interest, the MUSE4 phase consists of the coupling of a $PuO_2/UO_2 + Na$ core with an external neutron source of high intensity [1]. Coupling has been achieved by employing a specially constructed pulsed neutron generator called GENEPI, which produces monoenergetic neutrons either via a $D(d,n)^3He$ reaction (2.7 MeV neutrons) or a $T(d,n)^4He$ reaction (14.1 MeV neutrons). The measurements being undertaken in the MUSE4 program constitute an important experimental database to be used for validating the calculation methods and data employed in the analysis of ADS (e.g. ERANOS and its associated data libraries).

In this context, specific investigations were conducted to assess (via data sensitivity/uncertainty analyses) representativity between MUSE4 and emerging concepts of experimental accelerator-driven systems (XADS). For this purpose, simplified RZ models for MUSE4 and different current XADS designs with gas (He), Na and Pb/Bi coolants (XADS_He, XADS_Pb/Bi, XADS_Na) were set up. The fuel considered throughout, for MUSE4 as well as for all the XADS, is 23-25% enriched PuO_2/UO_2 MOX fuel of the type used for the second SUPERPHENIX core. For the analyses, the deterministic code system ERANOS (Version 2.0) was used. The parameters studied include: the multiplication factor k_{eff} , a spectral index, F_5/F_8 (the fission rate of ^{235}U relative to that of ^{238}U at the centre of the fuel region) and a spatial index, $F_{5,1}/F_{5,2}$ (the ^{235}U fission rate at the interface between spallation module and core midplane relative to that at the centre of the fuel zone).

Deterministic calculation scheme

General description of ERANOS

ERANOS-2.0 is a deterministic code system consisting of a variety of dedicated modules. In the present analysis, we use the cell code ECCO [2], the RZ transport theory code BISTRO [3] and first-order perturbation theory modules [4] in conjunction with the adjusted nuclear data library ERALIB-1 [5]. The numerical approximations are P1 for the anisotropy of scattering and S8 for the angular discretisation of the flux being computed in 33 energy groups. BISTRO solves the Boltzmann equation by means of a standard finite difference method.

Representativity factors and general approach

Employing a recently applied methodology with ERANOS [4], representativity factors r_{RE} between MUSE4 and the three XADS configurations (with He, Na and Pb/Bi coolants) were evaluated for integral parameters such as the multiplication factor k_{eff} and specific reaction rate ratios on the basis of first-order perturbation theory. These factors, which quantify the impact of nuclear data uncertainties on the prediction of I, the parameter of interest (depend on cross-sections P_1, \ldots, P_N), are obtained as follows.

Sensitivity coefficients S_i for $I(P_1, ..., P_N)$ are computed according to Eq. (1):

$$S_i = \frac{\Delta I}{I} / \frac{\Delta P_i}{P_i} \tag{1}$$

The relative uncertainty σ_I of I is obtained by using a covariance matrix D as shown in Eq. (2):

$$\sigma_I^2 = S^T D S \tag{2}$$

It should be noted that D is associated with a specific nuclear data library.

For the parameter I, the representativity factor r_{RE} between two systems (e.g. MUSE and a given XADS) is determined from Eq. (3) [4], the covariance matrix being taken from the adjusted data library ERALIB-1:

$$r_{RE} = \frac{S_{XADS}^{t} D_{ERALIB} S_{MUSE}}{\sqrt{(S_{XADS}^{t} D_{ERALIB} S_{XADS})(S_{MUSE}^{t} D_{ERALIB} S_{MUSE})}}$$
(3)

The value of r_{RE} lies between 0.0 and 1.0. The closer r_{RE} is to 1.0, the more representative is MUSE of the XADS.

Representativity factors can also be used to quantify the uncertainty reduction possible for the prediction of I on the basis of suitable integral measurements. This occurs via Eq. (4):

$$\sigma_{I,XADS_reduced}^2 = \sigma_{I,XADS}^2 \left(1 - \frac{r_{RE}^2}{1 + \sigma_{I,exp}^2 / \sigma_{I,MUSE}^2} \right)$$
(4)

Thereby, the experimental uncertainty of the parameter I [i.e. as measured in MUSE ($\sigma_{I,exp}$)] also plays a significant role. The smaller is the experimental uncertainty, the stronger is the uncertainty reduction for the predicted value of I in the system of interest, with the closeness of r_{RE} to 1.0 remaining an important aspect. Eq. (4) reflects the most optimistic case (zero experimental uncertainty):

$$\sigma_{I,XADS}^2 = \sigma_{I,XADS}^2 \left(1 - r_{RE}^2 \right) \tag{5}$$

In the current study, representativity between the MUSE4 experiments and the different XADS is evaluated based on the following scheme:

- 1. Assessment of nuclide-specific "integral sensitivities" on the basis of sensitivity coefficient (S_i) calculations [see Eq. (1)]. Integral sensitivity to a given nuclide is the uncertainty of I, which is obtained by assuming that a) there is no correlation between data for different nuclides, b) the individual reaction cross-sections for the nuclide considered are also not correlated and c) the relative uncertainty for each of the nuclide cross-sections is 100% over the whole energy range (< 20 MeV). Effectively, integral sensitivity is calculated on the basis of Eq. (2) while assuming that the matrix D is unity.</p>
- 2. Determination of the uncertainty of I with the correct covariance matrix D from ERALIB-1 [see Eq. (2)].

- 3. Calculation of the representativity factor r_{RE} [see Eq. (3)].
- 4. Determination of the reduced uncertainty [see Eqs. (4,5)].

The reason for currently using the adjusted data library ERALIB-1 is to avoid the well known dominating effect of ²³⁹Pu, which was observed in the analysis of MUSE3 in conjunction with the (unadjusted) JEF-2.2 library [4]. However, the resulting uncertainties may be somewhat small for the ADS situation, since the ERALIB adjustments were made solely on the basis of critical experiments. Also, it is necessary to underline the fact that method uncertainties, as well as uncertainties due to external source differences between MUSE4 and XADS, are not accounted for in the current analysis. Complementary studies, including method/data comparisons made in the framework of benchmark exercises, are certainly important in this context [6].

General description

Models

The simplified RZ models considered for XADS are based on current PDS-XADS designs [7]. These are described in Figure 1 and Table 1, where only the most important materials are indicated [8].

Figure 1. Definition of homogenised zones for three XADS models

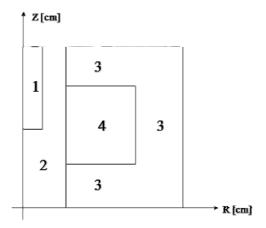


Table 1. Description of homogenised zones of three XADS models

Name	Zone 1	Zone 2	Zone 3	Zone 4
XADS_Pb/Bi	Void	Pb/Bi	Pb/Bi	$PuO_2/UO_2 + Pb/Bi$
XADS_He	Void	Pb/Bi	He + Steel	$PuO_2/UO_2 + He$
XADS_Na	Void	Pb/Bi	Na + Steel	$PuO_2/UO_2 + Na$

The basic principles for obtaining the models were that: a) the volume of the spallation source (void + Pb/Bi) and the volume of the fuel region (Zone 4) correspond to the PDS-XADS design, b) the outer radius of the reflector region (Zone 3) was adjusted to obtain a $k_{\rm eff}$ value of 0.97.

The reference experimental set-up considered is the second subcritical configuration investigated in the MUSE4 program, i.e. M4SC2 [8], the RZ model described in Figure 2 and Table 2. For the sake of consistency with XADS, the original outer radius of Zone 4 was modified slightly in order to achieve a $k_{\rm eff}$ value of 0.97.

Figure 2. Definition of homogenised zones for M4SC2 model

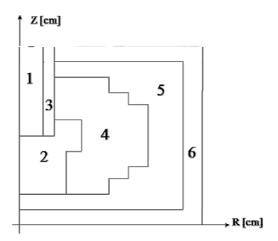


Table 2. Description of homogenised zones of M4SC2 model

Name	Zone 1	Zone 2	Zone 3	Zone 4	Zone 5	Zone 6
M4SC2	Void	Pb	Al	$PuO_2/UO_2 + Na$	Na + Steel	Steel

Parameters

As indicated earlier, representativity factors r_{RE} [see Eq. (3)] between M4SC2 and XADS_He, XADS_Na and XADS_Pb/Bi were considered for the three parameters listed below:

- 1. The multiplication factor k_{eff}.
- 2. F_5/F_8 , i.e. the fission of ^{235}U relative to that ^{238}U at the centre of the fuel region. This provides useful spectral information due to the different nature of ^{235}U and ^{238}U fission, the latter being a threshold reaction and the former not being a threshold reaction.
- 3. $F_{5,1}/F_{5,2}$, i.e. the ²³⁵U fission rate at the interface between spallation module and core midplane relative to that at the centre of the fuel zone. This spatial index is sensitive to the geometry and composition of the spallation module.

Numerical results and interpretation

Representativity for the multiplication factor k_{eff}

Relative "integral sensitivities" are presented in Table 3. It can be seen that the highest sensitivity in each case is to 239 Pu. The contributions of the other nuclides are much smaller and quite similar in magnitude, except for Pb_{nat} and 209 Bi, which have significant effects only in the XADS_Pb/Bi case.

 $K_{\rm eff}$ uncertainties (again, only due to nuclear data uncertainties) are presented in Table 4, the main contributing nuclides being indicated for each case.

Table 3. Relative integral sensitivities (%) of k_{eff} with respect to the main isotopes

Isotopes	M4SC2	XADS_Na	XADS_Pb/Bi	XADS_He
²³⁵ U	0.8	1.9	1.7	1.8
²³⁸ U	3.1	2.6	3.7	0.4
²³⁹ Pu	83.0	84.6	78.3	85.5
²⁴⁰ Pu	4.8	4.6	4.7	6.2
²⁴¹ Pu	1.6	4.6	4.1	4.4
⁵⁶ Fe	3.2	0.3	1.3	0.2
⁵² Cr	1.4	0.5	0.1	0.7
²³ Na	1.1	0.2	0.0	0.0
Pb _{nat}	0.0	0.1	2.8	0.1
²⁰⁹ Bi	0.0	0.1	3.0	0.1
Others	0.9	0.4	0.4	0.6

Table 4. Keff uncertainties associated with the ERALIB-1 library

Name	Uncertainty on the $k_{eff}(\sigma_I)$	Main contributors
M4SC2	± 162 pcm	⁵² Cr, ²³⁹ Pu, ⁵⁶ Fe
XADS_Na	± 163 pcm	²³⁹ Pu, ²⁴⁰ Pu, ⁵⁶ Fe
XADS_Pb/Bi	± 1 021 pcm	²⁰⁹ Bi, Pb _{nat} , ²³⁹ Pu
XADS_He	± 199 pcm	²³⁹ Pu, ⁵⁸ Ni, ²⁴⁰ Pu

The uncertainties are similar for M4SC2, XADS_Na and XADS_He (σ_I < 200 pcm), ²³⁹Pu being one of the main contributors in each configuration. The structural material isotope ⁵²Cr is a major contributor for M4SC2, due to the larger quantity of this nuclide in the experimental set-up as compared to the XADS. One also notes that the situation is completely different for the XADS_Pb/Bi case, where Pb_{nat} and ²⁰⁹Bi are the main contributors to the overall uncertainty (σ_I > 1 000 pcm) with the data for these nuclides not having been adjusted in ERALIB-1.

The corresponding representativity factors are provided in Table 5. It can be seen that for $k_{\rm eff}$ M4SC2 is quite representative of XADS_Na and XADS_He, the corresponding r_{RE} values being rather close to 1.0. On the contrary, the low presence of $Pb_{\rm nat}$ and the absence of ^{209}Bi in M4SC2 lead to a low-valued representativity factor for the XADS_Pb/Bi. This indicates the need for additional integral measurements related to the data of lead and bismuth.

Table 5. Representativity factors r_{RE} for k_{eff}

Compared systems	Representativity factor r_{RE}
$M4SC2 \leftrightarrow XADS_Na$	0.884
M4SC2 ↔ XADS_Pb/Bi	0.346
$M4SC2 \leftrightarrow XADS_He$	0.907

As indicated earlier, the degree to which the uncertainty of the prediction of a given parameter for an XADS can be reduced via an integral measurement depends on the corresponding representativity factor r_{RE} [see Eqs. (3,4)]. Thereby the experimental uncertainty associated with the measurement also plays a key role. To illustrate the point, Table 6 shows the k_{eff} uncertainty reduction for the case of the XADS_He, assuming different values of experimental uncertainty in M4SC2 [8].

Table 6. Example of k_{eff} uncertainty reduction for the XADS_He system

For the k _{eff} prediction	Value (with ERALIB-1)	
$\sigma_{I,XADS}$: Uncertainty for XADS_He	± 199 pcm	
$\sigma_{I,MUSE}$: Uncertainty for M4SC2 \pm 162 pcm		
r_{RE} : Representativity factor	0.907	
$\sigma_{I,XADS_reduced}$: Reduced uncertainty for XADS_He	177 mam	
(with an $\sigma_{I,exp}$ experimental uncertainty of ± 0 pcm)	± 77 pcm	
$\sigma_{I,XADS_reduced}$: Reduced uncertainty for XADS_He	± 127 nom	
(with an $\sigma_{I,exp}$ experimental uncertainty of \pm 100 pcm)	± 127 pcm	
$\sigma_{I,XADS_reduced}$: Reduced uncertainty for XADS_He	± 163 pcm	
(with an $\sigma_{I,exp}$ experimental uncertainty of ± 200 pcm)		

Once again, only uncertainties associated with nuclear data are being accounted for in the present analysis. Nevertheless, the sensitivity coefficients considered [see Eq. (1)] in determining corresponding representativity factors do allow the obtaining of important qualitative indications on the correlation between the compared systems. In the following sections, related to the two other integral parameters under consideration, the aspect of uncertainty reduction is not treated explicitly, the different XADS being compared with M4SC2 solely on the basis of integral sensitivities and representativity factors.

Representativity for F_5/F_8

The relative integral sensitivities to the main isotopes are given in Table 7 for the various cases. The contributions of 235 U and 238 U, these isotopes having a direct impact on the reaction rate ratio under consideration, are larger than in the previous (k_{eff}) case as expected. In addition, a significant contribution of 239 Pu is still observed for all the systems, while 23 Na, Pb_{nat} and 209 Bi have significant effects only in the systems in which they are present in an important way.

The corresponding representativity factors are given in Table 8. These are similar to the results for $k_{\rm eff}$. The subcritical core of M4SC2 is representative of XADS_Na and XADS_He. Again, the low representativity with respect to XADS_Pb/Bi reflects deficiencies associated with the data for Pb_{nat} and 209 Bi, as well as the low content of these nuclides in the experimental configuration.

Table 7. Relative integral sensitivities (%) of the spectral ratio F_5/F_8 to the main isotopes

Isotopes	M4SC2	XADS_Na	XADS_Pb/Bi	XADS_He
²³⁵ U	37.3	33.6	32.8	38.6
²³⁸ U	33.1	33.1	33.0	35.4
²³⁹ Pu	13.3	11.7	10.7	11.7
²⁴⁰ Pu	0.8	1.3	1.2	1.2
²⁴¹ Pu	0.2	0.5	0.5	0.5
⁵⁶ Fe	6.3	7.2	5.4	8.4
⁵² Cr	2.0	0.9	0.5	1.6
²³ Na	5.0	10.8	0.0	0.0
Pb _{nat}	0.4	0.1	6.8	0.2
²⁰⁹ Bi	0.0	0.1	8.5	0.2
Others	1.6	0.5	0.5	2.1

Table 8. Representativity factors r_{RE} for F_5/F_8

Compared systems	Representativity factor r_{RE}
$M4SC2 \leftrightarrow XADS_Na$	0.853
M4SC2 ↔ XADS_Pb/Bi	0.264
$M4SC2 \leftrightarrow XADS_He$	0.885

Representativity for $F_{5,1}/F_{5,2}$

Relative integral sensitivities for this spatial index are presented in Table 9. The contributions of the individual nuclides are significantly different from the previous two cases (see Tables 3 and 7), indicating the significant impact of the spallation module on this particular parameter. The contributions of Pb_{nat} and Pb_{nat} are Pb_{nat} and Pb_{nat} and Pb_{nat} and Pb_{nat} and Pb_{nat} are Pb_{nat} and Pb_{nat} and Pb_{nat} and Pb_{nat} and Pb_{nat} are Pb_{nat} and Pb_{nat} and Pb_{nat} are Pb_{nat} are Pb_{nat} and Pb_{n

As to be expected, the representativity factors given in Table 10 are also significantly different from the corresponding values in the previous sections. Generally speaking, the r_{RE} factors are much smaller. This is due to the different source regions, which are quite dissimilar in terms of geometry and material composition (e.g. the source module of M4SC2 has no 209 Bi as mentioned above). Additional calculations for the three XADS, which were carried out assuming modified targets where 209 Bi is replaced by Pb_{nat}, indeed yielded significantly larger representativity factors (shown in Table 10).

Table 9. Relative integral sensitivities (%) to the main isotopes for $F_{5,1}/F_{5,2}$

Isotopes	M4SC2	XADS_Na	XADS_Pb/Bi	XADS_He
²³⁵ U	0.2	0.3	0.3	0.1
²³⁸ U	34.5	15.7	22.4	15.9
²³⁹ Pu	20.9	5.5	1.0	6.0
²⁴⁰ Pu	4.9	3.5	5.9	1.3
⁵⁶ Fe	0.5	4.6	39.9	37.2
⁵⁷ Fe	0.6	2.3	6.2	4.9
⁵² Cr	3.8	3.2	1.4	0.1
⁵⁸ Ni	0.5	0.7	1.3	5.7
²³ Na	16.8	23.2	0.0	0.0
Pb _{nat}	15.3	20.7	15.0	15.0
²⁰⁹ Bi	0.0	19.0	4.8	13.4
Others	1.8	1.3	1.9	0.3

Table 10. Representativity factors r_{RE} for $F_{5,1}/F_{5,2}$

Compared systems	Rep. factor r_{RE}	Rep. factor r_{RE} (no ²⁰⁹ Bi in XADS spallation module)
M4SC2 ↔ XADS_Na	0.258	0.552
M4SC2 ↔ XADS_Pb/Bi	0.066	0.383
$M4SC2 \leftrightarrow XADS_He$	0.259	0.556

Conclusions

Investigations related to k_{eff} and reaction rate ratios were conducted to assess the representativity between MUSE4 and various concepts of experimental accelerator-driven systems (XADS). In this context, sensitivity/uncertainty calculations were performed using deterministic code system ERANOS (Version 2.0) in conjunction with its adjusted data library ERALIB-1 based on the JEF-2.2 evaluation. Employing a recently applied methodology [4], representativity factors r_{RE} between the second subcritical MUSE4 core (M4SC2) and the three current PDS-XADS designs (with He, Na and Pb/Bi coolants) were evaluated for different integral parameters.

Specifically, it was found that the representativity between M4SC2 and an XADS with an Na or He coolant is, in general, quite satisfactory except for the region with the source module. In the case of an XADS with Pb/Bi coolant, the relatively low representativity results from the large uncertainties associated with the nuclear data for Pb_{nat} and ²⁰⁹Bi, as does also the low content of these nuclides in the experimental configuration. This clearly indicates the need for additional integral experiments.

It is necessary to underline the fact that only data uncertainties were accounted for in the present study. Method uncertainties and combined method/data effects were not considered, nor were the effects of differences in the external neutron source [9]. Further investigations are called for in this context, for example detailed comparisons in the framework of specific benchmark exercises [6].

Acknowledgements

The authors would like to acknowledge the help provided by the EU PDS-XADS project team and the MUSE group of CEA/Cadarache in supplying various information related to the computational models employed.

REFERENCES

- [1] Soule, R., et al., "Neutronic Studies in Support of ADS: The MUSE Experiments in the MASURCA Facility", Accepted for publication in *Nuclear Science and Engineering* (2004).
- [2] Rimpault, G., "Algorithmic Features of the ECCO Cell Code for Treating Heterogeneous Fast Reactor Subassemblies", International Topical Meeting on Reactor Physics and Computations, Portland, USA (1995).
- [3] Palmiotti, G., et al., "Optimized Two-dimensional Sn Transport (BISTRO)", Nuclear Science and Engineering, 104-26 (1990).
- [4] Aliberti, G., *Caractérisation Neutronique des Systèmes Hybrides en Régimes Stationnaire et Transitoire*, Thèse de l'Université Louis Pasteur de Strasbourg (2001).

- [5] Fort, E., *et al.*, "Realisation and Performance of the Adjusted Nuclear Data Library ERALIB1 for Calculating Fast Reactor Neutronics", *Proceedings of PHYSOR'96*, Mito, Japan (1996).
- [6] Villamarin, D., *et al.*, "Benchmark on Computer Simulation of MASURCA Critical and Subcritical Experiments (MUSE4 Benchmark)", NEA/SEN/NSC/WPPT(2001)5, 2001.
- [7] "XADS Pb-Bi Cooled Experimental Accelerator Driven System Reference Configuration", Summary report, Ansaldo Energia SpA, ADS 1 SIFX 0500 (2001).
- [8] Plaschy, M., Études Numériques et Expérimentales de Caractéristiques d'un Système Rapide Sous-critique Alimenté par une Source Externe, Thèse de l'École Polytechnique Fédérale de Lausanne (EPFL), No. 2953 (2004).
- [9] Pelloni, S., "PDS-XADS LBE and Gas Cooled Concepts: Neutronic Parameters Comparisons", *Proceedings of PHYSOR'04*, Chicago, USA (2004).

THERMAL STABILITY OF THE U-Zr FUEL AND ITS INTERFACIAL REACTION WITH LEAD

B-S. Lee, Y. Kim, J-H. Lee, T-Y. Song

Korea Atomic Energy Research Institute P.O. Box 105, Yuseong, Daejeon, 305-600 Korea

Abstract

The effect of heat treatment on fuel rods at $630^{\circ}C$ and $700^{\circ}C$ and the interfacial reaction between fuel and lead were investigated. The U-Zr metallic fuel was fabricated by mixing, pressing, sintering and extrusion. There were two kinds of phases – α -Zr precipitates and a δ -UZr₂ matrix in the U-Zr metallic fuel. After heat treatment of the extruded rod at $630^{\circ}C$ and $700^{\circ}C$, the volume changes of the samples increased slightly and the density variation was negligible. Therefore, it is evident that U-Zr fuels have good thermal stability. The interface between U-55Zr fuel and Pb according to annealing time at $650^{\circ}C$ consisted of two distinctive regions – a reaction zone in the vicinity of the surface and an initial zone in the inner area. It should be noted that the thickness of the reaction zone was $26~\mu m$, $36~\mu m$ and $46~\mu m$ at 100~hrs, 200~hrs and 1~000~hrs, respectively. Also, the reaction zone consisted of an α -Zr layer and a Zr-depleted area.

Introduction

The blanket fuel assembly for HYPER (hybrid powder extraction reactor) contains a bundle of pins arrayed in a triangular pitch, which has a hexagonal bundle structure. The reference blanket fuel pin consists of the fuel slug of the TRU-xZr (x = 50-60 wt.%) alloy and is immersed in lead for thermal bonding with the cladding. The blanket fuel cladding material is ferritic-martensitic steel HT9.

Although there are lots of experimental data on the metallic alloys of U-Pu-Zr and U-Zr, they are for fuel types with a Zr fraction of less than 20 wt.%. Therefore, little data is available for the HYPER system fuel where the Zr fraction is higher than 30 wt.%. As a basic study on HYPER fuel, we fabricated U-55 wt.% Zr fuel instead of the actual TRU-Zr fuel. It appeared that no experimental data pertinent to the TRU-xZr (x = 50-60 wt.%) alloy existed. The U-55 wt.% Zr metallic fuel was fabricated by mixing, pressing, sintering and extrusion. This work was performed in order to investigate the microstructures and the thermal stability of the U55 wt.% Zr metallic fuel and the interfacial reaction between U-55 wt.% Zr fuel and Pb according to annealing time at 650° C.

Experimental procedure

The uranium powder was manufactured by a centrifugal atomiser and the zirconium powder (Sejong materials Co. Ltd, Korea) was prepared via the hydride-dehydride process.

The U-Zr metallic fuel was performed by mixing, pressing and sintering in optimum compaction and sintering conditions [1]. The sintered U-60 wt.% Zr was extruded by an indirect extrusion machine at 760°C and with a 13:1 extrusion ratio. Specimens of 25 mm in length were cut, vacuum-sealed in quartz tubes and annealed in a box furnace at 630°C and 700°C for up to 1 500 hrs. Sample swelling as a function of temperature and time was determined from dimensional changes. The densities of the annealed samples were calculated from the weights and dimensions. The microstructures and phase identification of the extruded rod and the annealed rod were examined by SEM and EDS. The area fraction of each phase obtained by SEM was analysed by a BMI plus ver. 4.0 (Winatech, Korea).

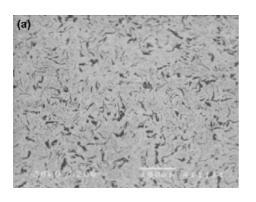
In order to clarify interfacial reaction between fuel and lead, a series of experiments were executed with fuel in Pb melt at 650°C for 100, 200 and 1 000 hrs. The composition of diffusion layers and the diffusion depth were analysed using SEM/EDS.

Results and discussion

Figure 1 shows uranium and zirconium particles. The mean particle sizes of the uranium and zirconium powders are $55 \mu m$ and $60 \mu m$, respectively. Most of the uranium particles have a smooth surface and a generally near-perfect spherical shape with a few attached satellites. On the other hand, the zirconium particles fabricated by the hydride-dehydride process have an irregular morphology.

Figure 2 shows the back-scattered electron (BSE) image of the sintered sample. As can be seen in phase diagrams, the α -Zr phases are distributed in the δ phase, which is observed as a white matrix [2]. Also, small amounts of pores are found throughout the sample.

Figure 1. Photographs of the atomised (a) U powder and (b) Zr powder



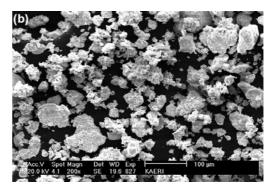
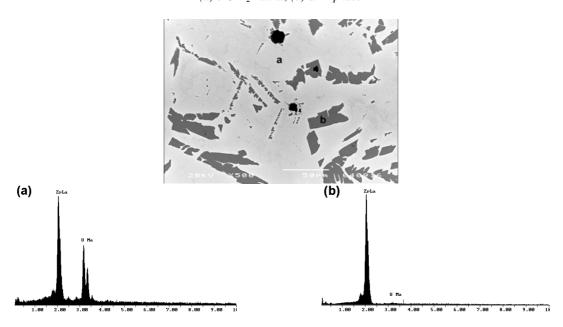


Figure 2. SEM micrograph and EDS analysis results for U-60 wt.% Zr sintered sample

(a) δ -UZr₂ matrix, (b) α -Zr phase

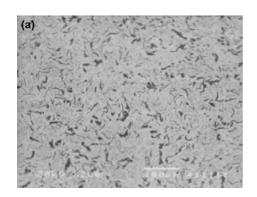


BSE images of the hot extruded rod are shown in Figures 3 and 4. In the sintered samples mentioned above, the α -Zr phases were also distributed (homogenously) in the white δ phase matrix and the porosity was drastically decreased because of the densification by the extrusion process. It was confirmed that the U-55 wt.% Zr alloy with a high melting point could be fabricated via a sintering process at a relatively low temperature in lieu of a conventional casting process.

Figure 5 shows the dependency of swelling behaviour and the density changes of temperature and time for the samples. The volume changes of the samples increased slightly and the density variation was negligible. Therefore, it is evident that U-55 wt.% Zr fuel has good thermal stability.

Figure 3. SEM micrographs of the extruded rod

(a) Transverse direction, (b) longitudinal direction



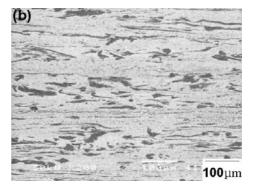


Figure 4. SEM micrograph and EDS analysis results for the extruded rod

(a) δ -UZ r_2 matrix, (b) α -Zr phase

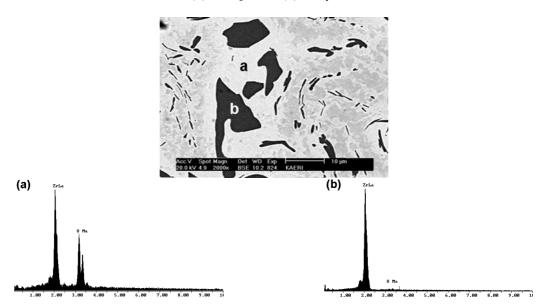
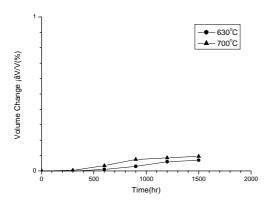


Figure 5. Volume and density changes of the extruded rod on temperature and time



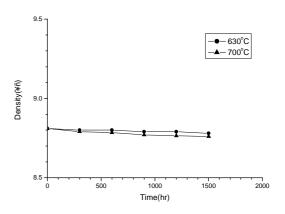


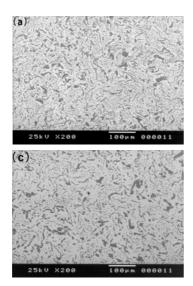
Figure 6 shows BSE images of the rod annealed at 630°C and 700°C for 600 hrs and 1 500 hrs. These figures show that as the annealing time increased, the lathed α -Zr phases began to break into pieces and grow into spherical particles. As the annealing temperature increased, spheroidising of the α -Zr phases was accelerated, with transformation to a spherical shape. We can interpret that the geometrically unstable lathed α -Zr phase transformed to the spherical phase with a lower surface area by coalescence. In addition, we think that the α -Zr and δ -UZr₂ phases dissolved and formed a solid solution at an annealing temperature above 617°C, and that the spheroidised α -Zr and δ phases appeared again during cooling.

As the annealing time increased, the hardness decreased and the decreasing rate of the hardness was much higher at 700°C than at 630°C (Figure 7). This is attributed to the increase of the area fraction of the δ phase and the decrease of the area fraction of the relatively hard α -Zr phase as the annealing temperature and time increased.

Figure 8 shows the area fraction of the α -Zr phase according to the annealing time at 630°C and 700°C. In the case of 630°C of annealing time, the area fraction of the α -Zr phase gradually decreased as the annealing time increased, whereas the area fraction of the α -Zr phase sharply decreased at the early stage of annealing time and then the decreasing rate declined at 700°C. This phenomenon agreed with the results on hardness values vis-à-vis annealing time as shown in Figure 7. When the U-55 wt.% Zr alloy is annealed at above 617°C, which is the unstable region of α -Zr phase, the alloy is diffused into the uranium matrix and finally forms δ phase at a lower temperature. Hence, it can be interpreted that the drastic decrease of area fraction of the α -Zr phase at the early stage of annealing time was due to the higher concentration gradient of Zr, which is the driving force of Zr diffusion.

Figure 6. SEM micrographs of the U-55 wt.% Zr fuel annealed at 630°C and 700°C for 600 hrs and 1 500 hrs

 $(a)(b) 630 \,\%, (c)(d) 700 \,\%, (a)(c) 600 \,hrs, (b)(d) \,1 \,500 \,hrs$



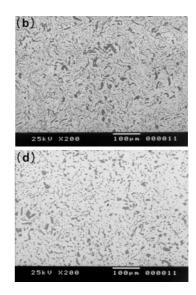


Figure 7. Variation of room temperature hardness of rods after annealing at 630°C and 700°C

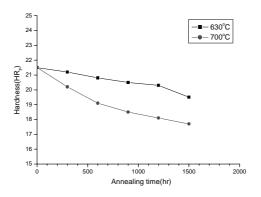


Figure 8. Variation of area fraction of α-Zr phase with annealing times at 630°C and 700°C

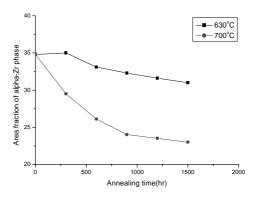


Figure 9 shows EDS line profile results on the interface between U-55Zr and Pb according to annealing time at 650°C. The microstructures of each sample consisted of two distinctive regions – a reaction zone in the vicinity of the surface and an initial zone in the inner area. It should be noted that the thickness of the reaction zone was 26 μ m, 36 μ m and 46 μ m at 100 hrs, 200 hrs and 1 000 hrs, respectively, as the annealing time increased. The reaction zone also consisted of two regions – an α -Zr layer and a Zr-depleted area. The α -Zr layer may be formed by a diffusivity difference between U and Zr atoms (i.e. Zr atom diffuses into the Pb melt during annealing while U is relatively intact due to lower diffusivity). The TRU in the metallic fuel is reported to react with stainless, as a cladding material then forms eutectic at a low temperature. Thus, it is anticipated that the α -Zr layer should effectively act as a reaction barrier with the cladding material.

In order to closely investigate the reaction layer, EDS analysis was performed as shown in Figure 10. The analysis shows that a negligible amount of Pb is present in the very outer layer of the reaction zone with Zr-rich phase (region A). And the α -Zr phase forms a thick layer of ~10 μ m underneath the surface (region B). Region C consists of U-rich phase and Zr formed by the decomposition of δ phase. As the annealing time increased, the thickness of the reaction layer from A to C increased to the direction of as-extruded area, region D.

Figure 9. Line profiles of interface of U-55Zr fuel with Pb bonding according to annealing time at $650^{\circ}C$

(a) 100 hrs, (b) 200 hrs, (c) 1 000 hrs

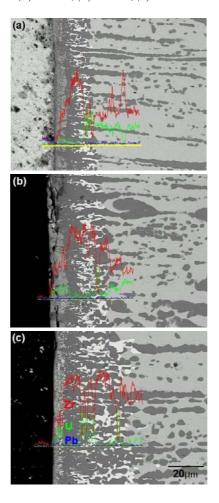
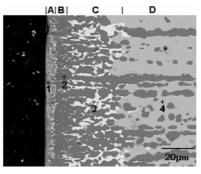


Figure 10. SEM/EDS results of U-55Zr with Pb bonding for 1 000 hrs at 650°C



Mark	Pb	U	Zr
1	0.76	19.11	80.13
2		0.37	99.63
3		95.11	4.89
4		31.82	68.18

Figures in at.%.

Conclusions

- The α -Zr phases were distributed in the white δ -UZr₂ phase matrix and the porosity was drastically decreased due to densification from the extrusion process.
- The volume changes of the samples increased slightly and the density variation was negligible. Therefore, it is evident that U-55 wt.% Zr fuel has good thermal stability.
- As annealing time increased, hardness decreased and the decreasing rate of hardness was much higher at 700°C than 630°C. This is attributed to the increase of area fraction of δ phase and the decrease of area fraction of relatively hard α -Zr phase as annealing temperature and time increased.
- The interface between U-55Zr fuel and Pb at annealing time and 650°C consisted of a reaction zone and an initial zone in the inner area. The reaction zone consisted of a α -Zr layer and a Zr-depleted area with thicknesses of 26 μ m (100 hrs), 36 μ m (200 hrs), 46 μ m (1 000 hrs).

REFERENCES

- [1] Cho, H.S., et al., Proceedings of the Korean Nuclear Society Spring Meeting, Jeju, Korea, May 2001.
- [2] Phase Transformation in Materials, 2nd Ed., D.A. Porter, K.E. Easterling (1992).

SUMMARIES OF TECHNICAL SESSIONS

Chairs: R. Sheffield, B-H. Choi

The summaries contained in this section reflect the views of the respective Chairperson(s) and do not necessarily reflect the views of the technical session group members.

SUMMARY OF TECHNICAL SESSION I: ACCELERATOR RELIABILITY

Chairs: A.C. Mueller, P. Pierini

A huge session – 11 contributions

ADS – Accelerator system designs (4)

- PDS-XADS reference accelerator, D. Vandeplassche.
- Japan SC ADS accelerator, N. Ouchi.
- LANL SC ADS accelerator, R. Garnett.
- FFAG at Kyoto University, M. Tanigaki.

Report on subcomponent operation (4)

- Spoke cavities, C. Mielot.
- China proton source + RFQ, X-L. Guan.
- PSI transport lines, P. Schmeltzbach.
- TRIPS source, G. Ciavola.

Beam dynamics aspects (2)

- Fault tolerance in RF and magnets, J.L. Biarrotte.
- Sensibility studies to errors, I. Shumakov.

Report on SNS commissioning (1), S. Henderson.

ADS accelerator design

Three out of four designs presented are based, to the largest possible extent, on a superconducting linac solution. *Is that a pattern?*

PDS-XADS

Explored cyclotron vs. linac capabilities.

- Performances, reliability, fault tolerance and extrapolation.
- Ruled out cyclotrons.

Designed a linac using reliability/availability guidelines.

- Technology chosen for injector (source + RFQ) and high energy section.
- Still a few options in intermediate energy stage.

Issuing "paper" deliverables but technological activities to present only supported by national programs.

JAERI-KEK

Today, the system design is slightly less developed (will need to further integrate availability issues) **YET** amazing technological effort has been made to provide real one-to-one components.

- Clear focus on development of SC cavity technology of bulk Nb electropolished cavities that drives most of the program choices.
- SC linac cryomodule test bench.
- Significant tests in near future.

LANL

All SC linac (after LEDA) fully based on spoke structures.

- Very sound beam dynamics studies.
- Work based on LANL spoke experience.
- Simpler 4 k operation. (Simplicity for reliability?)
- Looking towards 5-cell spokes. (We hope to hear about it!)

In the end 280 m/176 cavities, PDS-XADS has 250 m/190 cavities. Continuing the comparison is worthwhile.

FFAG

A concept from the 1950's (University consortium US) but feasible only as of today (complexity of B-fields). Actual intensities similar to synchrocyclotron (1 mA) but order of magnitude gain predicted. We need to have a comparative assessment following the guidelines of the HPPA3 report, which showed the limits of the reliability characteristics that can be achieved by a cyclotron vs. linac potential.

Subcomponent operation

Proton sources

There now exist at least four sources that clearly satisfy the ADS performance goals.

• [LEDA, SILHI], TRIPS and CIAE.

- Runs in 100-200 h range have confirmed high availability.
- Last thing to check long (three-month) runs.
- A priori, a twin-source design (PDS-XADS) seems acceptable.

RFQs

- LEDA operation record (more than needed for ADS).
- IPHI, CIAE status reported (we also have TRASCO). Big technological effort!
- Though none is currently operational.

PSI beam lines (0.2->2 mA)

Summary of about 20 years of HPPA beam line operation, including maintenance and reliability considerations.

Spoke cavities

- Tests have been reported with cavity exceeding ADS expectations.
- CNRS has a b = 0.15 under construction.
- Towards full engineering of a structure with all ancillary components (power coupler, CTS) a cyromodule is planned by CNRS.
- Importance of international access and collaboration around "regional" technological pole of excellence Ile de France SUPRATECH.

Beam dynamics aspects

Fault tolerance

- RF faults: can tolerate cavity loss (!) but need procedures for a fast reset of the linac to allow beam transmission, followed by a slower tuning to minimise beam losses.
- Magnet faults: the doublet focussing scheme (plus large linac SC cavity bore) can accept a full quadrupole doublet fault maintaining beam specs on target.

Sensitivity to fabrication tolerances

• Analytical and numerical methods can be used to assess the sensitivity to fabrication tolerances in devices such as RFQ or periodic beam lines.

SNS - A (pulsed) 1.4 MW SC proton HPPA

1 GeV 6% d.f., 1.4 mA average current (77% as of 01/2004)

Front end has been commissioned with beam.

• Source, RFQ, DTL 1-3 to 40 MeV, nominal parameters.

Installation and commissioning is steadily proceeding.

- Cavities tested with higher than expected gradients.
- DTL 4-6 and CCL 1-3 by August.
- Cryogenics system cooldown very soon.
- Start SC linac commissioning at the beginning of 2005.
- 81% energy gain from SC RF.
- Budget figures of interest for XADS.

Plan availability increase from 50% to 90% in five years.

We are eager to know the results of the SC linac commissioning.

Significant set-up that will demonstrate it is possible to transfer the digital RF controls used in TESLA to a SC proton machine.

- It is needed for the Lorentz force detuning of the pulsed cavities.
- Very important test bench for the path towards fault tolerance capabilities.

Long-term upgrade plan to 2-4 MW!

• Space already allocated for upgrade in high-beta section.

Conclusion

A lot of information and lessons learned from experimental accelerator development programmes in other fields of physics...

- ...but need for identified resources for XADS reliability programmes (US, Europe) and
- ...the availability/reliability requirements are unique for ADS.

Better situation in Asia (but present designs not optimised for fault tolerance).

SUMMARY OF TECHNICAL SESSION II: TARGET, WINDOW AND COOLANT TECHNOLOGY

Chairs: X. Cheng, T-Y. Song

"Research & Development on Lead-bismuth Technology for Accelerator-driven Transmutation System in JAERI" by Y. Kurata (JAERI), et al.

JAERI's corrosion loop (JLBL-1) test (350/400-450°C, 1 m/s).

- Corrosion depth of 316SS at high temperature part: \sim 100 μ m/3 000 h.
- At low temperature part: deposition of Pb/Bi and Fe-Cr, plugging (needed filter).

MES (Mitsui Engineering and Shipbuilding Co., Ltd.) loop (350-450°C, 0.4-0.6 m/s).

• 1.0×10^{-5} wt.% oxygen, 1 000 h, F82H/JPCA sample: no significant corrosion.

Static corrosion test (F82H, Mod. 9Cr-1Mo 316ss, etc.)

- 450° C, 3.2×10^{-4} wt.% oxygen, 3 000 h: increasing Cr \rightarrow decreasing corrosion depth.
- 550°C, 1.2×10^{-3} wt.% oxygen, 3 000 h: Si added steel shows good corrosion resistance.

"Vacuum Gas Dynamics Investigation and Experimental Results on the TRASCO-ADS Windowless Interface" by P. Michelato (INFN), et al.

- Windowless interface system is being developed as part of the TRASCO program. TRASCO program is to develop ADS. INFN, ENEA and Italian companies are involved in TRASCO.
- Pumping, vacuum and cold trap systems were investigated.
- LBE evaporation rate was measured and model was validated.
- Source terms of hydrogen isotopes and noble gases were investigated.
- Te was used for Po evaporation measurement and Hg experiment is under study.

"Corrosion Test in the Static Condition and Installation of Corrosion Loop at KAERI for Lead-bismuth Eutectic" by J-E. Cha (KAERI), et al.

KAERI installed Pb-Bi static corrosion test facility in 2003.

- Filtering samples for loop test.
- Oxygen control by H₂/H₂O, max. 800°C.
- Test performed at 650° C, $< 10^{-8}/10^{-6}$ wt.%, < 500 h for 316L/HT-9/T91.
 - Need to repeat the test to see consistency of data.

KAERI's corrosion loop.

- Completed design and fabrication of components in 2003.
- Plan to complete construction of the loop by September 2004.

"The Vacuum Interface Compatibility Experiment (VICE)" by P. Schuurmans (SCK•CEN), et al.

MYRRHA adopts windowless target system.

Problem: Gas/vapour emanation at windowless target surface.

- Outgassing.
- Spallation product.
- LBE evaporation.

VICE: Realistic geometry of lower beam line.

- Spallation product mix assessment was performed.
- Pre-conditioning vessel tested.
- Pb-Bi evaporation experiment performed.

"The Introduction of a Dual Injection Tube for the Design of a 20 MW Lead-bismuth Target System" by C-H. Cho (KAERI), et al.

DIT (dual injection tube) was introduced to improve KAERI's HYPER target design.

• Reduce target flow rate: lower pumping power, reduce thermal stripping.

Introduction of DIT (1 GeV, beam diameter 30 cm).

• Max. allowable beam current: 14 mA (parabolic), 21 mA (uniform).

Parabolic beam: smaller diameter of inner injection tube is recommended.

• Uniform beam: larger diameter of inner injection tube is recommended.

"Design Study Around Beam Window of ADS" by H. Oigawa (JAERI), et al.

Target and beam window design were performed for JAERI's ADS system.

• 1.5 GeV, Pb-Bi target, k_{eff} (0.97), 800 MWth.

A 30 MW beam was studied.

- Beam duct(45 cm), inlet temperature (300°C).
- Window: HCM12A (thickness: 2-4 mm).

Max. temperature of window outer surface: 490°C.

Max. stress: 106 MPa.

"Primary Isotope Yields for MSDM Calculations of Spallation Reactions on ²⁰⁸Pb with Proton Energy of 1 GeV" by S. Fan (CIAE), *et al.*

- MSDM code is a high-energy transport code used to simulate spallation reaction.
- Original MSDM code was modified to take into account effects related to level densities.
- After the modification, new calculation results turned out to agree with some experimental data of 1 GeV spallation reaction on a ²⁰⁸Pb target.
- But new MSDM results do not agree well when compared with the experimental data of neutron-rich nuclides.

"CFD Analysis on the Active Part of the Window Target Unit for LBE-cooled XADS" by N.I. Tak (FZK), et al.

CFD analysis was performed for XADS target.

- Target (Pb-Bi), natural convection cooling, inlet temperature (233°C).
- 600 MeV, 6 mA.

Steady-state case.

• Reduction in window thickness (at centre) to 2 mm leads to allowable max. temperature of outer window surface (limit: 500°C).

Transient case.

• At 1 s beam trip conditions, max. temperature drop is 207°C (412°C/s).

"Optimisation of a Code to Improve Spallation Yield Predictions in an ADS Target System" by T. Sawada (TIT), et al.

- PHITS: General purpose particle and heavy ion transport code system.
- Tried to optimize PHITS so that it can be used for ADS-related calculations with precision.

- Calculation prediction can be improved by:
 - Increasing the excited energy for the evaporation stage.
 - Reducing the pre-equilibrium stage.
 - Changing the timescale or cut-off energy for the intra-cascade stage.

SUMMARY OF TECHNICAL SESSION III: SUBCRITICAL SYSTEM DESIGN AND ADS SIMULATIONS

Chairs: W. Gudowski, H. Oigawa

Categories of presentations

- Research/demo facility design described or referenced to:
 - Kyoto, MYRRHA, TRADE.
- Conceptual design of full-scale transmuter:
 - Burn-up swing and CSMSR.
- Design of ADS components:
 - MYRRHA vessel studies, accelerator and BTL for TRADE.
- Benchmark on beam interruptions.

Research/demo facility design

- More international harmonisation would be beneficial for many parties (the same is valid for Pb/Bi technology experiments):
 - Similar experiments are under preparation or planned better focus and task distribution would be desirable (*probably not easy to agree upon*).
 - Real accelerators are going to be coupled with subcritical cores in the near future.
 - ADS, demo, PoP, etc. facilities should have clear objectives, *internationally harmonised*, in order to focus on investigation of important parameters for a real transmutation facility without unnecessary duplications.
 - > RACE experiment in US not reported.
 - > SAD (Russia, ISTC) not reported.

Conceptual design of full-scale transmuter

- Visible convergence for Pb/Bi system design concerning:
 - Power (800 MWth).
 - $K_{eff}(0.97)$.
 - Fuel options (nitride intensively studied but not exclusively).
- Big variety of core designs, we consider that there is great potential to optimise ADS performance.
- Variety of fuel compositions and fuel cycle.

- Fast information exchange between different groups is definitely beneficial for the progress of ADS concepts.
- Interesting alternative options for ADS under investigation; we would like to have a bit more clarity on CSMSR.

Design of ADS – components

Very interesting engineering work taking us closer to practical solutions.

• Even if the choice of accelerator is still an open question, it is clear that first PoP experiments will be done with cyclotron (Kyoto, TRADE, SAD, etc.).

Benchmark on beam interruptions

Easy conclusions:

- Everybody happy with benchmarks so time for validation activity.
- Time for an international *validation experiment*? Should it have been planned already? Can we use existing facilities? Should we take into account facilities under advanced planning/construction?
- Any role for OECD/NEA?

Final conclusions

- Interesting session covering very different topics with direct links to other sessions.
- Final recommendations/advice to participants and OECD/NEA should be done based on synthesis of all sessions.

SUMMARY OF TECHNICAL SESSION IV: SAFETY AND CONTROL OF ADS

Chairs: J-M. Lagniel, P. Coddington

Two papers – very design specific – were presented describing the results of WP2 of the PDS-XADS project and covering the two $\underline{80}$ XADS designs. The conclusions reached were: a) a Pb-Bi reactor ADS has significant safety characteristics, particularly if it has a low Δp and a high natural circulation flow rate, and b) a gas-cooled system has a short space period for beam-shut off end. Any pump-driven system will lie between these two.

We heard about the new Pb-Bi loop, which provides neutral circulation, etc., and is useful for only Pb-Bi system.

An interesting paper was presented describing a proposal for dynamic control of an ADS by linking.

The intriguing use of void boxes with mini cycles to control reactivity swings was discussed as well as plans to look at burnable poisons.

A paper compared the PDS-ADS Pb-Bi 80 MW and the reactor design considered as part of the EU FUTURE project.

- This has oxide fuels with Am and Cm, leading to different fuel thermal properties and reduced ≥/ and large positive void worth.
- Compensation results presented for TOP.
 - UTOP results sensitive to fuel properties providing small in comparison to the subcriticality level. Power change is the same.
 - ULOF because of high subcriticality margin. Power remains ~1.0 so response is function of flow reduction, i.e. system behaviour.
- Results are sensitive to the change in fuel thermal properties.

SUMMARY OF TECHNICAL SESSION V: ADS EXPERIMENTS AND TEST FACILITIES

Chairs: P. D'hondt, V. Bhatnagar

Summary

- Five (5) papers were presented.
- One (1) paper was not presented: "Core Neutronics Assessment for TRADE Experiments" by D.G. Naberezhnev, *et al.* (ANL, USA).

Paper 1

- Presented by H. Oigawa (JAERI, Japan).
- Entitled "Concept of Transmutation Experimental Facility".
- Remarks within the J-PARC complex:
 - TEF-P: Physics experiments with MA nitride fuel (600 MeV, 10 W), H⁻ beam as a mock-up of subcritical facility.
 - Validation of neutronics, performance test of ADS and transmutation of MA and LLFP.
 - TEF-T: Material irradiation tests (200 kW beam, dia. = 4 cm, 10¹⁴ n/cm²/s) in flowing LBE without nuclear fuel.
 - Test lifetime of window, structural material under (n, p) irradiation, compatibility of materials with LBE, operation and control of spallation target system
 - Decision and operation 2008 onwards?

Paper 2

- Presented by M. Hron (NRI, Czech Republic).
- Entitled "Experimental Verification of Selected Transmutation Technology and Materials for Basic Components of a Demonstration Transmuter with Liquid Fuel Based on Molten Fluorides".
- Remarks:
 - **SPHINX**: spent hot fuel incinerator by neutron flux project.
 - Accelerator-driven concept of MA transmutation demonstrator with molten salt using dry processing.
 - BLANKA 1: fluoride material testing probe irradiated in research reactor at NRI, Rez (T, p measurements).
 - BLANKA 4: Larger assembly also installed.
 - EC project: MOST and Russian AMPULA.

Paper 3

- Presented by Y.H. Kim (KAERI, Korea).
- Entitled "Application of the HYPER System to the DUPIC Fuel Cycle".
- Remarks:
 - DUPIC: PWR spent fuel recycled in CANDU reactor after a simple refabrication process.
 - After pyroprocessing, this spent fuel can be transmuted in HYPER system.
 - Proliferation resistance cycle, uranium resource saving.
 - Fuel cycle cost comparable to once-through cycle.
 - HYPER system preliminary design features and performance analysis presented.
 - Utilities still have to show interest in this cycle.

Paper 4

- Presented by P. Coddington (PSI, CH).
- Entitled "Numerical Comparisons Between Neutronic Characteristics of MUSE4 Configurations and XADS-type Models".
- Remarks:
 - Aim was to make representativity calculations between MUSE4 and XADS concepts for Na, He and LBE-cooled systems.
 - Results do not show good representation in LBE case.
 - There were comments from the audience regarding the utility of the calculations as configurations do not match.
 - Pb-loaded MUSE4 system could be better for these calculations.
 - Suggestion for TRADE simulation was made but not found to be of great value.

Paper 5

- Presented by B.S. Lee (KAERI, Korea).
- Entitled "Reaction of Pb Bonding Between Fuel and Cladding".

• Remarks:

- Presentation included the fabrication process and a study of thermal stability of U-Zr fuel.
- U-55 wt.% Zr fuel has good thermal stability.
- A significant interaction between U-55 wt.% Zr and Pb is observed at 650°C.
- Thickness of the interaction zone is 26, 36, 46 μm when the sample is immersed in liquid Pb for 100, 200, 1 000 hrs, respectively.

SUMMARIES OF WORKING GROUP DISCUSSION SESSIONS

Chairs: R. Sheffield, B-H. Choi

The summaries contained in this section reflect the views of the respective Chairperson(s) and do not necessarily reflect the views of the working group members.

SUMMARY OF WORKING GROUP DISCUSSION ON ACCELERATORS

Chair: P.K. Sigg

Discussion

Suggestions (Y.L. Cho) on chosen topics – availability, reliability, high intensity and efficiency:

- Define *observation period*; Suggestion (A. Mueller): For three months of operation, followed by one month shutdown period (maintenance, restocking).
 - Comment (T. Mukaiyama): For future industrial applications (burners), observation period should be greater than one year!

Beam trips: Neglect events $< 1 \text{ sec.} \rightarrow \text{goal: only five trips/month,} > 1 \text{ sec.}!$

• Comment (R. Sheffield): Trip of > 10 sec. \rightarrow reactor will shut down!

Reliability culture: Suggestion is to go to industrial standards (e.g. aerospace industry).

- Comment (P. Schmelzbach): There is a trade-off between system complexity and redundancy!
- Definition (P. Pierini): Differentiate component vs. system reliability; this should be clearly identified in specs.
- Comment: Recording (data logging) is not sufficient → (H. Aït Abderrahim, A. Mueller) interpretation is essential, affects the quality of the available database.

Suggestion: Agree upon/introduce common standards or guidelines! (But WHO will do that?)

- Comment: Safety increases reliability (!?)
- Comment (R. Sheffield): Diagnostics can be failure cause false alarms can be frequent (see P. Schmelzbach).
- Comment (several speakers): Aside from well known "trouble areas" (vacuum, RF systems), many interruptions are caused by support system failures (power grid, cooling systems, etc.), and are not directly influenced by accelerator design).
- Observation: Many machines are "experimental", that is to say, prototypes (one of a kind), so reliability is not the same as in industrial plants (including reactors).
- Comment (D. Vandeplassche): Commercial cyclotrons (e.g. for medical applications) are "finished" at one time → *no more tinkering*!

Energy efficiency; Question (T. Mukaiyama): Can anyone give a number for overall electrical efficiency?

- Discussion: You can expect a maximum of ~50% (based on several opinions R. Sheffield, A. Mueller...)
- Comment (R. Sheffield): There exists a trade-off between availability and efficiency → redundancy (like hot spares) is detrimental to energy efficiency!

Question (L. Ponomarev): What amount of beam power is desired for ADS? Or, how much power can reactors reasonably take? (The question has been asked before.)

Answer (H. Aït Abderrahim, A. Mueller, others): 10-20 MW is sufficient!

Non-technical issues

Funding: What can be done to increase funding for ADS? On the accelerator side (A. Mueller), accelerator community seems to get short changed. Suggestion: Widen the spectrum of applications offered for accelerator development!

Manpower: There seems to be a shortage of qualified, experienced accelerator scientists. Question: What can be done to alleviate the problem in view of the increasing demand for new/existing projects?

Suggestions: More aggressive advertising in universities, career planning, etc. More effort is needed!

Conclusion

Questions yet to be resolved (T. Mukaiyama): After having worked out solutions to some of the key questions (such as: what accelerator type is "best" \rightarrow try SC linac; what are the costs \rightarrow first estimates available for prototype machines; what is the energy consumption \rightarrow see above discussion on energy efficiency), there are still a few open questions. At present, trying to answer them is only guesswork. Typically, questions such as "When will what accelerator be fully operational?" and "When will the trip rate reach the desired value?" are still waiting to be answered in the future. The prototypes now under construction will help us in providing answers to these questions and many smaller issues.

SUMMARY OF WORKING GROUP DISCUSSION ON SUBCRITICAL SYSTEMS AND INTERFACE ENGINEERING

Chair: W. Gudowski

What are the expected results of our discussion?

- Understanding where we are internationally with ADS programmes and to clarify the details.
- Understanding to where different projects are heading.
- Finding synergies and benefits in international collaboration and a good balance between COMPETITION and COLLABORATION.
- Agreement on what message we should convey to nuclear utilities and to the nuclear community as a whole on ADS and P&T issues.
- Some important technical issues not yet answered:
 - What is the maximum beam power accepted by a reactor? (Reactor perspective is not only beam trips!)
- Advise OECD/NEA on priorities in its P&T and ADS activities.

${f Good\ starting\ point\ -\ conclusions\ of\ M.\ Salvatores'\ presentation\ regarding\ putting\ an\ international\ perspective\ on\ the\ future\ of\ ADS}$

"The perceived role of P&T has evolved from an optional strategy aiming to reduce the burden on deep geological storage, to an integral component of future nuclear systems. In this new perspective, 'transmutation' is achieved in an optimum manner in a fast neutron reactor, with the homogeneous recycling of not separated TRU."

The main reactions to this statement are:

- The perception by the geological disposal community is not in line with the statement especially perceived in EURADWASTE 2004. P&T is perceived for the moment as a burden for geological disposal. Thus, there is a real need for communication between the two communities.
- In an electricity market open for competition it will be difficult to make a dirty fuel cycle acceptable to the utilities. **This will be jeopardizing the competitiveness of nuclear electricity generation** (one of the Gen. IV criteria).
- Multiple recycling needed within P&T is unacceptable to utilities as considered in the homogeneous burning.
- Transmutation is achieved in an optimum manner in a fast neutron system, be it a critical reactor or an ADS system.

"Specialized devices, like ADS, can have a role in a transition scenario between the present LWR-dominated to a future FR-dominated situation."

The main reactions to this statement are:

- ADS is a dedicated system for waste burning but not simply for the transition period between the LWR era and the FR-dominated era. **ADS will be a dedicated waste burner also when the FR will be deployed for economical reasons**.
- Even if ADS will be for a transition period, this will be a long one (around one century).
- Why such a huge effort for a transition period if limited to 20 to 30 years as claimed by the Gen. IV community?

"In any case, ADS deployment can hardly be considered by a single country in isolation and a 'regional' approach is needed, where countries with rather different policies in terms of nuclear power development can join efforts to develop shared facilities."

The main reactions to this statement are:

- This is true at the Asian level as a Japan-China-Korea initiative has begun to join the effort related to the R&D support programme for ADS and even to join the effort for ADS facilities in the J-PARC ADS part (the latest statement on the wishes of Japan; enlargement to world collaboration).
- A joint effort in R&D support can also be achieved through the ISTC initiatives.
- This is true at European level under the EC FP (4, 5, 6) programmes for R&D support but a step further would be needed in terms of realisation.

Target issues

"The best solution issue – window or windowless."

The main reactions to this statement are:

- Windowless can be a favoured design under the condition that after a hydraulic demonstration and a vacuum interface compatibility demonstration, the realisation of an experimental testing is realised.
- Scale 1/1 experiment is needed.
- If windowless can be accepted, one should not avoid a cold window to protect the accelerator from eventual contamination.
- The technology of cold windows, even used in other applications, needs to be demonstrated at the high-power proton beams considered for ADS accelerators.

- An assessment of the maximum power acceptable in the windowless design should be established.
- The optimum acceptable proton energy for ADS application is 600 to 800 MeV; thus one cannot relax more on the energy to avoid high currents.

"Can we envisage an experiment in the near future to help us resolve this issue? A WINDOWLESS MEGAPIE? Where and when?"

The main reactions to this statement are:

- Yes such an experiment should be prepared and performed.
- An attempt was done during the FP6 project IP EUROTRANS but due to budget shorting this is not taken in the present programme.
- PSI and SCK•CEN are thinking about such an experiment.

"Too little work has been done on the consequences of a window break."

The main reactions to this statement are:

• For the first time, work on this topic has been reported by JAERI and the group recommends an increase in this effort.

SUMMARY OF WORKING GROUP DISCUSSION ON SAFETY AND CONTROL OF ADS

Chair: P. Coddington

Points of discussion

We thought of a good idea to propose to OECD/NEA/NSC. There should be a safety-related benchmark to follow the beam trip benchmark.

- Eight-hundred (800) MW transmuters with Pb-Bi coolant with **MA load** fuel and typical beta, reactivity, **k**_{eff}.
- Both at beginning and end of cycle.
- Also during hot standby conditions.

Safety activities

Licensing challenge.

Subcritical:

New concept	Length of time to get CSR	> ABWR
New coolant		> AP600/AP1000
New fuel		

Do not try all three at once.

Safety guideline – DEC

Core melt – DEC

Two realistic analyses of core melt/recriticality is thought too difficult (at this time) to analyse.

Therefore, the **core melt frequency** needs to be so low to be in the residual risk category.

- For **detectable** transients, if beam trip is the only barrier then the failure rate needs to be 10⁸.
- For **undetectable** transients, these have to be designed out. For example, open core design from JAERI to avoid SA blockages.

Safety

Much discussion

ADS offers advantages over critical systems for **reactivity accidents**.

However, beam trip (without shutdown system) is the first and only shutdown mechanism.

- All system transients/design must be analysed to define GRACE PERIOD for beam shut off to determine:
 - Nature and location response of detection system for all possible accidents.
 - Processing logic.
 - Definition of signal that goes to the accelerator.

All this needs a high reliability since this may be the only barrier to **core melt**.

This means that a review needs to be made on **safety-related instrumentation**.

Temperature increases:

- Thermocouples where/each SA, core exit.
- Response time core exit problems with flow mixing, etc.
- Power monitor.
- Subcriticality monitor.

For DBs - safety guidelines

Goal – no off-site release. Based on analysis of PDS-XADS, there will be limited clad failures.

But this is **not obvious** since we saw for the gas reactor. DBs may lead to pin failure and therefore activity release to the containment.

This will then help to define the requirements for the **containment** – an issue **not discussed**.

ADS reactivity control

Shutdown

Discussion relating to an alternative shutdown mechanism.

Conclusion that a **set of "safety" shutdown rods** should be considered, these being most relevant when k_{eff} becomes close to 1.0.

Burn-up control

Discussion on the presentations:

- Use of burnable poisons.
- Limited use of control rods.
- Void boxes (for mini cycles).
- Link to the beam power, to the core power.
- Generally, there are safety considerations for constant (fixed) beam power.

Definition of optimum subcriticality level

This needs to be better quantified rather then left to guesswork and big margin.

Annex 1

LIST OF WORKSHOP ORGANISERS

Honorary co-chairs

Luis Echávarri, Director-General of OECD/NEA Chung-Won Cho, Director-General of Nuclear Energy, Ministry of Science and Technology (Korea)

General co-chairs

Byong-Ho Choi, Director, High Power Proton Accelerator Development, KAERI (Korea) Richard Sheffield, Los Alamos National Laboratory (USA)

Scientific secretary

Byung-Chan Na (OECD/NEA)

International scientific advisors

Richard Sheffield (LANL, USA), Chair

Pierre D'hondt (SCK•CEN, Belgium)

Yves Jongen (IBA, Belgium)

Alex Mueller (CNRS Orsay, France)

Dominique Warin (CEA, France)

Guy Laffont (CEA, France)

Jean-Marie Lagniel (CEA, France)

Concetta Fazio (FZK, Germany)

Guenter Bauer (FZJ, Germany)

Joachim Knebel (FZK, Germany)

Alberto Negrini (Ansaldo, Italy)

Carlo Pagani (INFN, Italy)

Stefano Monti (ENEA, Italy)

Hideki Takano (JAERI, Japan)

Minoru Takahashi (Tokyo Institute of Technology, Japan)

Nobuo Ouchi (JAERI, Japan)

Yuji Kurata (JAERI, Japan)

Byong-Ho Choi (KAERI, Korea)

Tae-Yung Song (KAERI, Korea)

Won-Seok Park (KAERI, Korea)

Dolores Gomez-Briceno (CIEMAT, Spain)

Enrique Gonzalez (CIEMAT, Spain)

Marcus Eriksson (RIT, Sweden)
Waclaw Gudowski (RIT, Sweden)
Thomas Stammbach (PSI, Switzerland)
Colin Zimmerman (BNFL, UK)
David Hill (ORNL, USA)
Eric Pitcher (LANL, USA)
George Lawrence (LANL, USA)
Jordi Roglans (ANL, USA)
Michael Cappiello (LANL, USA)
Phillip Finck (ANL, USA)
Kemal Pasamehmetglu (LANL, USA)
Rusi P. Taleyarkhan (ORNL, USA)

Local organising committee

In-Soo Ko, POSTECH, local organising committee Chair Yong-Sub Cho, KAERI Sang-Hoon Nam, Pohang Accelerator Laboratory (PAL) Seung-Jeong Noh, Dankook University Moo-Hyun Cho, POSTECH Yong-Seok Hwang, Seoul National University Jong-Bum Choi, Chonbuk National University Sung-Oh Cho, KAIST Jae-Hyung You, KAERI Won-Seok Park, KAERI Tae-Yung Song, KAERI Chang-Sup Lee, KEPRI Seong-Man Bae, KEPRI Jae-Won Park, KAERI, local organising committee Co-ordinator

Annex 2

LIST OF PARTICIPANTS

BELGIUM

AÏT ABDERRAHIM, Hamid

Tel: +32 14 33 22 77

SCK•CEN, Reactor Physics & Myrrha Dept.

200 Boeretang

B-2400 MOL

Tel: +32 14 33 22 77

Fax: +32 14 32 15 29

Eml:haitabde@sckcen.be

 D'HONDT, Pierre
 Tel: +32 14 33 22 00

 SCK◆CEN
 Fax: +32 14 32 15 29

 Boeretang 200
 Eml:pdhondt@sckcen.be

 B-2400 MOL
 Eml:pdhondt@sckcen.be

HAECK, Wim

SCK◆CEN

Boeretang 200

B-2400 MOL

Tel: +32 14 33 22 71

Fax: +32 14 32 15 29

Eml: whaeck@sckcen.be

VANDEPLASSCHE, Dirk
IBA, Chemin du Cyclotron 3
B-1348 LOUVAIN-LA-NEUVE
Tel: +32 10 47 58 49
Fax: +32 10 47 58 47
Eml:dirk@iba.be

CHINA (PEOPLE'S REPUBLIC OF)

FAN, Sheng

China Institute of Atomic Energy

P.O. Box 275 (41)

BEIJING 102413

Tel: +86 10 693 57 670

Fax: +86 10 693 57 008

Eml:sfan@iris.ciae.ac.cn

GUAN, Xialing

China Institute of Atomic Energy
Institute of High Energy Physics

Tel: +86 10 693 58 804
Fax: +86 10 693 57 787
Eml:guanxl@mail.ihep.ac.cn

P.O. Box 918 BEIJING 100039

 HAN, Yinlu
 Tel: +86 10 693 57 275

 China Institute of Atomic Energy
 Fax: +86 10 693 57 787

 P.O. Box 275-41
 Eml:han@iris.ciae.ac.cn

BEIJING 102413

LI, Jigen China Institute of Atomic Energy P.O. Box 275-56

BEIJING 102413

SHI, Yongqian Tel: +86 10 693 58 028 China Institute of Atomic Energy Fax: +86 10 693 57 787 P.O. Box 275-45 Eml:shiyq@iris.ciae.ac.cn

Tel: +86 10 693 58 284

Fax: +86 10 693 57 787

Eml:jigen@iris.ciae.ac.cn

Eml:Pavel.Hosnedl@skoda-js.cz

BEIJING 102413

Tel: +86 10 693 58 798 XIA, Haihong China Institute of Atomic Energy Fax: +86 10 693 57 787 P.O. Box 275-80 Eml:xiahh@iris.ciae.ac.cn

BEIJING 102413

CZECH REPUBLIC

HOSNEDL, Pavel Tel: +420 6 05 22 16 66 SKODA Nuclear Machinery Ltd. Fax: +420 3 78 04 27 49

Orlik 266

CZ-316 06 PLZEN

HRON, Miloslav Joseph Tel: +420 7 28 53 01 92 Nuclear Research Institute Rez, plc Fax: +420 2 66 17 23 98 Eml:hron@nri.cz

CZ-250 68 REZ

Tel: +420 6 02 18 59 44 PEKA, Ivo Fax: +420 2 66 17 23 98 Nuclear Research Institute

Rez 130 Eml:hro@ujv.cz

CZ-250 68 REZ

FRANCE

BOKOV, Pavel Tel: +33 1 69 08 78 47 **CEA Saclay** Fax: +33 1 69 08 75 84 Eml:pavel.bokov@cea.fr

DSM/DAPNIA/SPhN Bât. 703

F-91191 GIF-SUR-YVETTE

LAGNIEL, Jean-Michel Tel: +33 1 69 26 52 49

CEA DAM Fax: +33 1 69 26 70 24 DPTA-SP2A, BP 12 Eml: jean-michel.lagniel@cea.fr

F-91680 BRUYÈRES-LE-CHÂTEL

MIÉLOT, Christophe Tel: +33 1 69 15 71 27 Fax: +33 1 69 15 77 35 **IPN Orsay**

IPNO Bât. 106, 15 rue G. Clémenceau Eml:mielot@ipno.in2p3.fr

F-91406 ORSAY CEDEX

MIÉLOT-WIRATKASEM, Worachina Tel: +33 1 69 15 71 27 5 rue G. Clémenceau Fax: +33 1 69 15 77 35

F-91406 ORSAY Eml:worachina@yahoo.com MUELLER, Alex Dept. Head, R&D Accelerators/Exotic Beams

Institut de Physique Nucléaire Bât. 106, 15 rue G. Clémenceau F-91406 ORSAY CEDEX

Tel: +33 1 69 15 62 40 Fax: +33 1 69 15 77 35 Eml:mueller@ipno.in2p3.fr

SALVATORES, Massimo Tel: +33 4 42 25 33 65 Commissariat à l'Énergie Atomique Fax: +33 4 42 25 41 42 Eml:massimo.salvatores@cea.fr

DEN/DIR/AFF-INT Bldg. 101 CEA Cadarache

F-13108 SAINT-PAUL-LEZ-DURANCE

GERMANY

CHEN, Xue-Nong Tel: +49 72 47 82 59 85 Fax: +49 72 47 82 38 24 Forschungszentrum Karlsruhe Eml:xchen@iket.fzk.de

Inst. for Nuclear and Energy Technologies Hermann-von-Helmholtz-Platz 1

D-76344 EGGENSTEIN-LEOPOLDSHAFEN

CHENG, Xu Tel: +49 72 47 82 48 97 Fax: +49 72 47 82 48 37 Forschungszentrum Kalrsruhe

Inst. for Nuclear and Energy Technologies Eml:xu.cheng@iket.fzk.de

Hermann-von-Helmholtz-Platz 1 D-76344 EGGENSTEIN-LEOPOLDSHAFEN

INDONESIA

MUKAIYAMA, Takehiko Tel: +62 21 570 7571 Director, Jakarta Liaison Office Fax: +62 21 570 7577

Japan Atomic Industrial Forum, Inc. MidPlaza 1, 12th Floor Eml:mukaiyamat@biz.net.id

JL. Jend. Sudirman Kav. 10-11

JAKARTA 10220

ITALY

BURGAZZI, Luciano Tel: +39 051 60 98 556 FIC-NUC ENEA Fax: +39 051 60 98 279

Via Martiri di Monte Sole, 4 Eml:burgazzi@bologna.enea.it

I-40129 BOLOGNA

CIAVOLA, Giovanni Tel: +39 095 54 22 62 Group Leader Fax: +39 095 54 23 02 Istituto Nazionale de Fisica Nucleare – LNS Eml:celona@lns.infn.it

Via S. Sofia, 44 I-95123 CATANIA

Tel: +39 049 806 85 01 COMUNIAN, Michele Fax: +39 049 806 88 29 **INFN-Legnaro National Laboratories**

Viale dell'universita, 2 Eml:michele.comunian@lnl.infn.it

I-35020 Legnaro, PADOVA

FAGOTTI, Enrico INFN-LNL Viale dell'universita, 2 I-35020 Legnaro, PADOVA Tel: +39 049 806 84 13 Fax: +39 049 806 88 29 Eml:enrico.fagotti@lnl.infn.it

MICHELATO, Paolo INFN-Milano-LASA Via Fratelli Cervi, 201 I-20090 Segrate, MILANO Tel: +39 02 503 19 562 Fax: +39 02 503 19 543

Eml: Paolo. Michel ato@mi.infn.it

PICARDI, Luigi ENEA Via E. Fermi, 45 I-00044 FRASCATI Tel: +39 069 40 05 774 Fax: +39 069 40 05 334 Eml:picardi@frascati.enea.it

PIERINI, Paolo INFN-Milano-LASA Via Fratelli Cervi, 201 I-20090 Segrate, MILANO Tel: +39 02 23 92 560 Fax: +39 02 23 92 543 Eml:paolo.pierini@mi.infn.it

JAPAN

KOBAYASHI, Hiroshi Tokyo Institute of Technology N1-459, Ninokata Laboratory 2-12-1 Ookayama Megro Tel: +81 3 5734 3062 Fax: +81 3 5734 3062

Eml:hkobayas@geo.titech.ac.jp

KURATA, Yuji Nuclear Transmutation Group Center for Neutron Science, JEARI Tokai-mura, Naka-gun, Ibaraki-ken 319-1195 Tel: +81 29 282 5059 Fax: +81 29 282 6489

Eml:ykurata@popsvr.tokai.jaeri.go.jp

MISAWA, Tsuyoshi Research Reactor Institute Kyoto University Kumatori, Sennan, Osaka 590-0494 Tel: +81 724 51 2376 Fax: +81 724 51 2603

Eml:misa@kuca.rri.kyoto-u.ac.jp

MISHIMA, Kaichiro Research Reactor Institute Kyoto University Kumatori-cho, Sennan-gu, Osaka 590-0494

Tel: +81 724 51 2449 Fax: +81 724 51 2637

Eml:mishima@rri.kyoto-u.ac.jp

NISHIHARA, Kenji Center for Neutron Science, JAERI 2-4 Shirakata-shirane Tokai-mura, Naka-gun, Ibaraki-ken 319-1195 Tel: +81 029 282 6935 Fax: +81 029 282 5671

Tel: +81 29 864 5230

Eml:nishi@omega.tokai.jaeri.go.jp

NOGUCHI, Shuichi KEK Accelerator Laboratory 1-1 Oho Tsukuba-shi, Ibaraki-ken 305-0801

Fax: +81 29 864 3182 Eml:shuichi.noguchi@kek.jp OIGAWA, Hiroyuki
Tel: +81 29 282 6935
Nuclear Transmutation Group
Fax: +81 29 282 5671
Center for Proton Acc. Facilities, JAERI
Eml:oigawa@omega.tokai.jaeri.go.jp

Center for Proton Acc. Facilities, JAERI Tokai-mura, Ibaraki-ken 319-1195

OUCHI, Nobuo Tel: +81 29 282 5461 Accelerator Group, JAERI Fax: +81 29 282 5663

Tokai-mura, Naka-gun, Ibaraki-ken 319-1195 Eml:ouchi@linac.tokai.jaeri.go.jp

Eml:tanigaki@rri.kyoto-u.ac.jp

TAKANO, Hideki Tel: +81 29 282 6151 Deputy Director Fax: +81 29 282 5996

Center of Neutron Science, JAERI Eml:takano@cens.tokai.jaeri.go.jp

Tokai-mura, Naka-gun, Ibaraki-ken 319-1195

TANIGAKI, Minoru Tel: +81 724 51 2476 Research Reactor Institute Fax: +81 724 51 2620

Kyoto University 2-1010 Asashiro-nishi Kumatori-cho, Sennan-gun

KOREA (REPUBLIC OF)

BAE, Young-Soon Tel: +82 54 279 1136

POSTECH Fax:

San 31, Hyoja-Dong Eml:ysbae7@postech.ac.kr

Namgu, POHANG 790-784

CHA, Jae-Eun

Tel: +82 42 868 2065

HYPER Team, KAERI

Fax: +82 42 868 2080

P.O. BOX 105

Eml:jecha@kaeri.re.kr

Yuseong, DAEJEON 305-600

CHAI, Jong-Seo Tel: +82 11 9132 2239

KIRAMS Fax:

215-4 Gongneung-Dong Eml:jschai@kcch.re.kr

Nowon-Ku, SEOUL 139-709

 CHANG, In-Soon
 Tel: +82 42 868 82 46

 President, KAERI
 Fax: +82 42 861 75 21

 150 Duckjin-Dong
 Eml:ischang@kaeri.re.kr

Yuseong, DAEJEON 305-353

CHO, Chung-Ho

KAERI

P.O. Box 105

Tel: +82 42 868 2914

Fax: +82 42 868 2080

Eml:ex-chcho@kaeri.re.kr

Yuseong, DAEJEON 305-600

CHO, Yong-Sub Tel: +82 42 868 2975

KAERI Fax:

P.O. Box 105 Eml:choys@kaeri.re.kr

CHOE, Wonho Tel: +82 42 869 2539

KAIST Fax:

373-1 Kusong-Dong Eml:wcho@kaist.ac.kr Yuseong, DAEJEON 305-701

CHOI, Byung-Ho Tel: +82 02 2299 1732

KAERI Fax:

150 Duckjin-Dong Eml:bhchoi@kaeri.re.kr

Yuseong, DAEJEON 305-353

CHOI, Han-Woo Tel: +82 42 868 3664

KIGAM Fax

30 Gajeong-Dong Eml:starlove@kigam.re.kr

Yuseong, DAEJEON 305-350

CHOI, M. Tel: +82 11 9902 9619

KISTI Fax:

52 Eoeun-Dong Eml:mcho@reseat.re.kr

Yuseong, DAEJEON 305-353

GIL, Choong-Sup

Tel: +82 42 868 8104

Nuclear Engineering Dept., KAERI

P.O. Box 105

Tel: +82 42 868 8104

Fax: +82 42 868 8103

Eml:csgil@kaeri.re.kr

Yuseong, DAEJEON 305-600

GWON, Saang-Won Tel: +82 2 503 7651

Ministry of Science & Technology (MOST) Fax:

Government Complex Eml:swgwon@most.go.kr

Gwacheon City, Gyeonggi-Do 427-715

JANG, Ji-Ho Tel: +82 42 868 8952

KAERI Fax:

150 Duckjin-Dong Eml:jangjh@kaeri.re.kr

Yuseong, DAEJEON 305-353

JOO, Po-Kook Tel: +82 42 868 82 73 Project Manager Fax: +82 42 861 11 84

Ind. Technology Coop. Grp., KAERI Eml:

P.O. BOX 105

Yuseong, DEAJEON 305-600

JUNG. II-Lae Tel: +82 42 868 8036

KAERI Fax:

150 Duckjin-Dong Eml:ex-jil714@kaeri.re.kr

Yuseong, DAEJEON 305-353

 JUNG, Ki-Jung
 Tel: +82 42 868 2060

 Director
 Fax: +82 42 861 1015

Planning Division, KAERI Eml:kjjung@kaeri.re.kr P.O. Box 105

JUNG, Y.S. Tel: +82 42 365 2115

RLC Networks Inc. Fax:

111-5 Eoeun-Dong Eml: yssystems@hanmir.com

Yuseong, DAEJEON 305-807

KIM, Bo-Young Tel: +82 42 868 2998

KAERI Fax

P.O. Box 105 Eml:ex-midas@kaeri.re.kr

Yuseong, DEAJEON 305-600

KIM, Do-Heon Tel: +82 42 868 8651 Nuclear Data Evaluation Laboratory Fax: +82 42 868 2636 KAERI Eml:kimdh@kaeri.re.kr

P.O. Box 105

Yuseong, DAEJEON 305-600

KIM, Hee-Soo Tel: +82 02 995 2974

Dankook University Fax:

147 Hannam-Dong Eml:kong010@hotmail.com

Hougsan, SEOUL 140-714

KIM, Hyung-Duk Tel: +82 42 868 8133

KAERI Fax:

150 Duckjin-Dong Eml:ex-hdgim@kaeri.re.kr

Yuseong, DAEJEON 305-353

KIM, In-Gyu Tel: +82 42 868 8031

KAERI Fax:

P.O. Box 105 Eml:igkim@kaeri.re.kr

Yuseong, DAEJEON 305-600

KIM, Jae-Keun Tel: KAERI Fax:

P.O. Box 105 Eml:ex-kjg@kaeri.re.kr

Yuseong, DAEJEON 305-600

KIM, Jaehang Tel: +82 2 970 1357

KIRAMS Fax:

215-4 Gongneung-Dong Eml:jhkim68@kcch.re.kr

Nowon, SEOUL 139-709

KIM, Joonkon Tel: +82 42 868 3663

KIGAM Fax:

30 Gajeong-Dong Eml:kimacc@kigam.re.kr

Yuseong, DAEJEON 305-350

KIM, Jun-Yeon Tel: KAERI Fax:

P.O. Box 105 Eml:jykim2@kaeri.re.kr

KIM, K.P. Tel: +82 42 868 2747

KAERI Fax:

P.O. Box 105 Eml:KPKIM@kaeri.re.kr

Yuseong, DEAJEON 305-600

KIM, Kye-Ryung Tel: +82 42 868 8602

KAERI Fax

P.O. Box 105 Eml:kimkr@kaeri.re.kr

Yuseong, DAEJEON 305-600

KIM, Mi-Hye Tel: +82 42 868 2836

KAERI Fax:

150 Duckjin-Dong Eml:ex-namihy@kaeri.re.kr

Yuseong, DAEJEON 305-353

 KIM, Seong-Yun
 Tel: +82 42 868 2126

 KAERI
 Fax: +82 42 861 8292

 150 Duckjin-Dong
 Eml:sykim@kaeri.re.kr

Yuseong, DAEJEON 305-353

KIM, Yonghee Tel: +82 42 868 2067

KAERI Fax:

P.O. Box 105 Eml:yhkim@kaeri.re.kr

Yuseong, DAEJEON 305-600

KIM, Yong-Hwan Tel: KAERI Fax:

P.O. Box 105 Eml:ex-yhkim@kaeri.re.kr

Yuseong, DAEJEON 305-600

KIM, Yong-Nam Tel: +82 02 2299 1732

Department of Nuclear Engineering Fax:

Hanyang University Eml:captin@nural.hanyang.ac.kr

17 Haengdang-Dong

Sungdong, SEOUL 133-791

KIM, Yu-Seok Tel: +82 02 970 1364

KAERI Fax:

P.O. Box 105 Eml:unison@kcch.re.kr

Yuseong, DAEJEON 305-600

KOH, S.K. Tel: +82 52 259 2321

Ulsan University Fax:

San 29, Muger 2-Dong Eml:skkoh@ulsan.ac.kr

ULSAN 680-749

KONG, Young-Jo Tel: +82 02 995 29 74

Dankook University Fax

147 Hannam-Dong Eml:0010k@hanmail.net

Hougsan, SEOUL 140-714

KWON, Hyeok-Jung Tel: +82 42 868 86 65

KAERI Fax:

P.O. Box 105 Eml:hjkwon@kaeri.re.kr

Yuseong, DAEJEON 305-600

KWON, Hyuk-II Tel: +82 42 868 28 10

KAERI Fax:

P.O. Box 105 Eml:hikwon@kaeri.re.kr

Yuseong, DAEJEON 305-600

 LEE, Bong-Sang
 Tel: +82 42 868 29 71

 KAERI
 Fax: +82 42 868 20 80

 P.O. Box 105
 Eml:ex-lbs@kaeri.re.kr

Yuseong, DAEJEON 305-600

LEE, Chan-Young Tel: +82 42 868 89 53

KAERI Fax:

P.O. Box 105 Eml:ex-ley@kaeri.re.kr

Yuseong, DAEJEON 305-600

LEE, Hwa-Ryun Tel: +82 42 868 28 81

KAERI Fax:

150 Duckjin-Dong Eml:ex-hrlee@kaeri.re.kr

Yuseong, DAEJEON 305-353

LEE, Jae-Hyung Tel: +82 42 868 29 11

KAERI Fax:

P.O. Box 105 Eml:jhlee3@kaeri.re.kr

Yuseong, DAEJEON 305-600

LEE, Jae-Sang Tel: +82 42 868 27 94

KAERI Fax:

P.O. Box 105 Eml:jslee8@kaeri.re.kr

Yuseong, DAEJEON 305-600

LEE, Il-Soo Tel: +33 1 44 05 24 10 First Secretary Fax: +33 1 47 55 86 70 Delegation of the Rep. of Korea to OECD Eml:islee@most.go.kr

2-4, rue Louis David 75782 PARIS CEDEX 16

LEE, Sang-Hee Tel: +82 42 868 87 34

KAERI Fax:

P.O. Box 105 Eml:ex-leesh@kaeri.re.kr

Yuseong, DAEJEON 305-600

LEE, Seok-Kwan Tel: +82 02 792 60 81

Dankook University Fax:

147 Hannam-Dong Eml: Vodcall@lycos.co.kr

Hougsan, SEOUL 140-714

LEE, Seok-Ki Tel: +82 42 868 87 40

KAERI Fax:

P.O. Box 105 Eml:ex-sklee@kaeri.re.kr

Yuseong, DAEJEON 305-600

LEE, Seung-Hyun Tel: +82 42 868 87 41

KAERI Fax: P.O. Box 105 Eml:

Yuseong, DAEJEON 305-600

LEE, Soo-Yeon Tel: +82 42 868 22 80

KAERI Fax:

P.O. Box 105 Eml:ex-syli22@kaeri.re.kr

Yuseong, DAEJEON 305-600

LEE, Young-II Tel: +82 41 857 56 55

KAERI Fax:

P.O. Box 105 Eml:Mutanty@korea.com

Yuseong, DAEJEON 305-600

MIN, Kyoung-Wook Tel: +82 42 869 25 25

KAIST Fax:

373-1 Kusong-Dong Eml:kwmin@space.kaist.ac.kr

Yuseong, DAEJEON 305-701

NAM, J.W. Tel: +82 42 868 89 58

KAERI Fax:

P.O. Box 105 Eml:ex-jwnam@kaeri.re.kr

Yuseong, DAEJEON 305-600

NO, Yong-Oh Tel: KAERI Fax:

P.O. Box 105 Eml:ex-siren746@kaeri.re.kr

Yuseong, DAEJEON 305-600

NOH, Seung-Jung Tel: Dankook University Fax:

147 Hannam-Dong Eml:snjoj@dankook.ac.kr

Hougsan, SEOUL 140-714

PARK, Jae-Won
Proton Engineer Frontier Project
Fax: +82 868 29 70
Fax: +82 868 81 31
KAERI
Eml:ex-pjw@kaeri.re.kr

150 Duckjin-Dong

Yuseong, DAEJEON 305-353

PARK, Mi-Young Tel: +82 42 868 89 52

KAERI Fax

P.O. Box 105 Eml:ex-mypark@kaeri.re.kr

PARK, Mum-Sik Tel: +82 42 868 28 82

KAERI Fax:

P.O. Box 105 Eml:ex-bspark@kaeri.re.kr

Yuseong, DAEJEON 305-600

PARK, Won-Seok
Tel: +82 42 868 83 75
Head of Project Operation Team
Nuclear Hydrogen Prod. Project, KAERI
Fax: +82 42 868 20 80
Eml:wonpark@kaeri.re.kr

P.O. Box 105

Yuseong, DAEJEON 305-600

SANG, Hyo-Han Tel: +82 42 868 27 16

KAERI Fax:

P.O. Box 105 Eml:twios96@hananet.net

Yuseong, DAEJEON 305-600

SEOL, Kyung-Tae Tel: +82 02 970 13 64

KAERI Fax:

P.O. Box 105 Eml:unison@kcch.re.kr

Yuseong, DAEJEON 305-600

SHIM, Chan-Bo Tel: KAERI Fax:

P.O. Box 105 Eml:ex-ldshim@kaeri.re.kr

Yuseong, DAEJEON 305-600

SHIN, Min-Jae Tel: KAERI Fax:

P.O. Box 105 Eml:ex-mjshin@kaeri.re.kr

Yuseong, DAEJEON 305-600

SHIN, Uncheol Tel: +82 19 406 14 55

KIPO, Government Complex – Daejeon Fax:

Dunsan-Dong Eml:sinuc1@kipo.go.kr

Seo-Gu, DAEJEON 302-701

SOHN, Chang-Won Tel: +82 42 868 29 98

KAERI Fax:

P.O. Box 105 Eml:ex-cwsohn@kaeri.re.kr

Yuseong, DAEJEON 305-600

 SONG, Tae-Yung
 Tel: +82 42 868 89 24

 KAERI
 Fax: +82 42 868 20 80

 P.O. Box 105
 Eml:tysong@kaeri.re.kr

Yuseong, DAEJEON 305-600

SONG, Young-Ki Tel: +82 42 868 85 92

KAERI Fax:

P.O. Box 105 Eml:ygsong@kaeri.re.kr

YANG, D.Y. Tel: +82 2 332 60 11

Kepco Fax:

58-2 Sungsan-Dong Eml:kepyang@prosyscon.co.kr

Mapo, SEOUL 121-250

YANG, Maeng-Ho Tel: +82 42 868 21 50

KAERI Fax:

P.O. Box 105 Eml:mhyang@kaeri.re.kr

Yuseong, DAEJEON 305-600

YOO, Ki-Suk Tel: +82 2 332 60 11

Pro-System Fax:

58-2 Sungsan-Dong Eml:ksyoo111@yahoo.co.kr

Mapo, SEOUL 121-250

YOON, Dae-Soo Tel:
Director-General Fax:
Ministry of Science & Technology (MOST) Eml:

Government Complex – Gwacheon Gwacheon City, Gyeonggi-Do 427-715

RUSSIAN FEDERATION

DEGTYAREV, Alexey M. Tel: +7 095 196 9530 Head of Laboratory Fax: +7 095 196 7270 RRC Kurchatov Institute Eml:amd@nsi.kiae.ru

Nuclear Safety Institute

Kurchatov Sq. 1 MOSCOW 123182

PONOMAREV, Leonid Tel: +7 095 947 2772 RCC MUCATEX Fax: +7 095 947 2787

ul. Rogova 9-2 Eml:mucatex.leonid@g23.relcom.ru

MOSCOW 123098

SHUMAKOV, Igor Tel: +7 095 315 6313
Head of Linear Accelerator Department Fax: +7 095 314 1053
Moscow Radiotechnical Institute (MRTI) Eml:ishumakov@mtu-net.ru

Warshawskoe shosse, 132

MOSCOW 117519

SWEDEN

GUDOWSKI, Waclaw Tel: +46 8 5537 82 00/73 656 0887

Nuclear and Reactor Physics Fax: +46 8 5537 84 65 Royal Institute of Technology Eml: wacek@neutron.kth.se

Center for Physics, Astronomy and Biotech

Roslagstullsbacken 21 S-106 91 STOCKHOLM

SWITZERLAND

CODDINGTON, Paul Tel: +41 56 310 27 38 Lab. for Reactor Physics & System Behaviour Fax: +41 56 310 23 27

Paul Scherrer Institute Eml:Paul.Coddington@psi.ch CH-5232 VILLIGEN - PSI

GROESCHEL, Friederich Tel: +41 56 310 21 96 Alternate TG Metal Member Fax: +41 56 310 31 31

Head Sect. Str. Mat. & Corrosion Eml:friedrich.groeschel@psi.ch

Paul Scherrer Institute, WHGA/246 CH-5232 VILLIGEN - PSI

SCHMELZBACH, Pierre A. Tel: +41 56 310 40 73 Fax: +41 56 310 33 83 Head of the Accelerator Division

Paul Scherrer Institute, WBGA/C22 Eml:Pierre.Schmelzbach@psi.ch

CH-5232 VILLIGEN - PSI

SIGG, Peter Tel: +41 56 310 32 34 Head, RF Section Fax: +41 56 310 32 94 Paul Scherrer Institute, WLGA/C25 Eml:peter.sigg@psi.ch

CH-5232 VILLIGEN - PSI

UNITED STATES OF AMERICA

Argonne, IL 60439

Tel: +1 630 252 6616 CHO, Yanglai

Argonne National Laboratory

9700 S. Cass Ave. Eml:yc@aps.anl.gov

HENDERSON, Stuart D. Tel: +1 865 241 6794 Accelerator Physics Group Leader Fax: +1 865 574 6617

Spallation Neutron Source Project Eml:shenderson@sns.gov 701 Scarboro Road Oak Ridge, TN 37830

SHEFFIELD, Richard Tel: +1 505 667 1237 Los Alamos National Laboratory Fax: +1 505 667 7443 LANSCE-DO, MS H851 Eml:sheff@lanl.gov

Los Alamos, NM 87545

INTERNATIONAL ORGANISATIONS

BHATNAGAR, Ved Tel: +32 2 299 58 96 **European Commission** Fax: +32 2 299 49 91

Nuclear Fission & Radiation Protection Eml: Ved.Bhatnagar@cec.eu.int

DGRTD J.4, CDMA 1/46 **B-1049 BRUSSELS**

MARCUS, Gail H.

Deputy Director-General

OECD Nuclear Energy Agency
12 boulevard des Iles
F-92130 ISSY-LES-MOULINEAUX

Tel: +33 1 45 24 10 02
Fax: +33 1 45 24 11 10
Eml:gail.marcus@oecd.org

NA, Byung Chan
OECD Nuclear Energy Agency, Data Bank
12 boulevard des Iles
F-92130 ISSY-LES-MOULINEAUX
Tel: +33 1 45 24 10 91
Fax: +33 1 45 24 11 28
Eml:na@nea.fr

OECD PUBLICATIONS, 2, rue André-Pascal, 75775 PARIS CEDEX 16

PRINTED IN FRANCE

(66 2005 15 1) – No. 54409 2005

OECD, 1999.

Software: 1987-1996, Acrobat is a trademark of ADOBE.

All rights reserved. OECD grants you the right to use one copy of this Program for your personal use only. Unauthorised reproduction, lending, hiring, transmission or distribution of any data or software is prohibited. You must treat the Program and associated materials and any elements thereof like any other copyrighted material.

All requests should be made to:

Head of Publications Service, OECD Publications Service, 2, rue André-Pascal, 75775 Paris Cedex 16, France.

OCDE, 1999

Logiciel, 1987-1996, Acrobat, marque déposée d'ADOBE.

Tous droits du producteur et du propriétaire de ce produit sont réservés. L'OCDE autorise la reproduction d'un seul exemplaire de ce programme pour usage personnel et non commercial uniquement. Sauf autorisation, la duplication, la location, le prêt, l'utilisation de ce produit pour exécution publique sont interdits. Ce programme, les données y afférantes et d'autres éléments doivent donc être traités comme toute autre documentation sur laquelle s'exerce la protection par le droit d'auteur.

Les demandes sont à adresser au :

Chef du Service des Publications, Service des Publications de l'OCDE, 2, rue André-Pascal, 75775 Paris Cedex 16, France.

TABLE OF CONTENTS

Foreword		3
Executive Summ	ary	11
Welcome		15
	D-S. Yoon Congratulatory Address	17
	I-S. Chang Welcome Address	19
	G.H. Marcus OECD Welcome	21
GENERAL SES	SSION: ACCELERATOR PROGRAMMES AND APPLICATIONS	23
	CHAIRS: B-H. CHOI, R. SHEFFIELD	
	T. Mukaiyama Background/Perspective	25
	M. Salvatores Accelerator-driven Systems in Advanced Fuel Cycles	27
	S. Noguchi Present Status of the J-PARC Accelerator Complex	37
	H. Takano R&D of ADS in Japan	45
	R.W. Garnett, A.J. Jason Los Alamos Perspective on High-intensity Accelerators	57
	J-M. Lagniel French Accelerator Research for ADS Developments	69
	T-Y. Song, J-E. Cha, C-H. Cho, C-H. Cho, Y. Kim, B-O. Lee, B-S. Lee, W-S. Park, M-J. Shin Hybrid Power Extraction Reactor (HYPER) Project	81

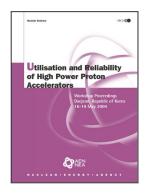
	V.P. Bhatnagar, S. Casalta, M. Hugon Research and Development on Accelerator-driven Systems in the EURATOM 5 th and 6 th Framework Programmes	89
	S. Monti, L. Picardi, C. Rubbia, M. Salvatores, F. Troiani Status of the TRADE Experiment	101
	P. D'hondt, B. Carluec The European Project PDS-XADS "Preliminary Design Studies of an Experimental Accelerator-driven System"	113
	F. Groeschel, A. Cadiou, C. Fazio, T. Kirchner, G. Laffont, K. Thomsen Status of the MEGAPIE Project	125
	P. Pierini, L. Burgazzi ADS Accelerator Reliability Activities in Europe	137
	W. Gudowski ADS Neutronics	149
	P. Coddington ADS Safety	151
	Y. Cho Technological Aspects and Challenges for High-power Proton Accelerator-driven System Application	153
TECHNICAL S	ESSION I: ACCELERATOR RELIABILITY	163
	CHAIRS: A. MUELLER, P. PIERINI	
	D. Vandeplassche, Y. Jongen (for the PDS-XADS Working Package 3 Collaboration) The PDS-XADS Reference Accelerator	165
	N. Ouchi, N. Akaoka, H. Asano, E. Chishiro, Y. Namekawa, H. Suzuki, T. Ueno, S. Noguchi, E. Kako, N. Ohuchi, K. Saito, T. Shishido, K. Tsuchiya, K. Ohkubo, M. Matsuoka, K. Sennyu, T. Murai, T. Ohtani, C. Tsukishima Development of a Superconducting Proton Linac for ADS	175
	C. Miélot Spoke Cavities: An Asset for the High Reliability of a Superconducting	173
	Accelerator; Studies and Test Results of a β = 0.35, Two-gap Prototype and its Power Coupler at IPN Orsay	185
	X.L. Guan, S.N. Fu, B.C. Cui, H.F. Ouyang, Z.H. Zhang, W.W. Xu, T.G. Xu Chinese Status of HPPA Development	195

	J.L. Biarrotte, M. Novati, P. Pierini, H. Safa, D. Uriot Beam Dynamics Studies for the Fault Tolerance Assessment of the PDS-XADS Linac	203
	P.A. Schmelzbach High-energy Beat Transport Lines and Delivery System for Intense Proton Beams	215
	M. Tanigaki, K. Mishima, S. Shiroya, Y. Ishi, S. Fukumoto, S. Machida, Y. Mori, M. Inoue Construction of a FFAG Complex for ADS Research in KURRI	217
	G. Ciavola, L. Celona, S. Gammino, L. Andò, M. Presti, A. Galatà, F. Chines, S. Passarello, XZh. Zhang, M. Winkler, R. Gobin, R. Ferdinand, J. Sherman Improvement of Reliability of the TRASCO	
	Intense Proton Source (TRIPS) at INFN-LNS	223
	R.W. Garnett, F.L. Krawczyk, G.H. Neuschaefer An Improved Superconducting ADS Driver Linac Design	235
	A.P. Durkin, I.V. Shumakov, S.V. Vinogradov Methods and Codes for Estimation of Tolerance in Reliable Radiation-free High-power Linac	245
	S. Henderson Status of the Spallation Neutron Source Accelerator Complex	257
TECHNI	ICAL SESSION II: TARGET, WINDOW AND COOLANT TECHNOLOGY	265
	CHAIRS: X. CHENG, T-Y. SONG	
	Y. Kurata, K. Kikuchi, S. Saito, K. Kamata, T. Kitano, H. Oigawa Research and Development on Lead-bismuth Technology for Accelerator-driven Transmutation System at JAERI	267
	P. Michelato, E. Bari, E. Cavaliere, L. Monaco, D. Sertore, A. Bonucci, R. Giannantonio, L. Cinotti, P. Turroni Vacuum Gas Dynamics Investigation and Experimental Results on the TRASCO ADS Windowless Interface	279
	J-E. Cha, C-H. Cho, T-Y. Song Corrosion Tests in the Static Condition and Installation of Corrosion Loop at KAERI for Lead-bismuth Eutectic	291
	P. Schuurmans, P. Kupschus, A. Verstrepen, J. Cools, H. Ait Abderrahim The Vacuum Interface Compatibility Experiment (VICE) Supporting the MYRRHA Windowless Target Design	301
	-	

C-H. Cho, Y. Kim, T-Y. Song Introduction of a Dual Injection Tube for the Design of a 20 MW Lead-bismuth Target System	313
H. Oigawa, K. Tsujimoto, K. Kikuchi, Y. Kurata, T. Sasa, M. Umeno, K. Nishihara, S. Saito, M. Mizumoto, H. Takano, K. Nakai, A. Iwata Design Study Around Beam Window of ADS	325
S. Fan, W. Luo, F. Yan, H. Zhang, Z. Zhao Primary Isotopic Yields for MSDM Calculations of Spallation Reactions on ²⁸⁰ Pb with Proton Energy of 1 GeV	335
N. Tak, H-J. Neitzel, X. Cheng CFD Analysis on the Active Part of Window Target Unit for LBE-cooled XADS	343
T. Sawada, M. Orito, H. Kobayashi, T. Sasa, V. Artisyuk Optimisation of a Code to Improve Spallation Yield Predictions in an ADS Target System	355
SESSION III: SUBCRITICAL SYSTEM DESIGN AND TIONS	363
CHAIRS: W. GUDOWSKI, H. OIGAWA	
T. Misawa, H. Unesaki, C.H. Pyeon, C. Ichihara, S. Shiroya Research on the Accelerator-driven Subcritical Reactor at the Kyoto University Critical Assembly (KUCA) with an FFAG Proton Accelerator	365
K. Nishihara, K. Tsujimoto, H. Oigawa Improvement of Burn-up Swing for an Accelerator-driven System	373
S. Monti, L. Picardi, C. Ronsivalle, C. Rubbia, F. Troiani Status of the Conceptual Design of an Accelerator and Beam Transport Line for Trade	383
A.M. Degtyarev, A.K. Kalugin, L.I. Ponomarev Estimation of some Characteristics of the Cascade Subcritical Molten Salt Reactor (CSMSR)	303
F. Roelofs, E. Komen, K. Van Tichelen, P. Kupschus, H. Aït Abderrahim CFD Analysis of the Heavy Liquid Metal Flow Field	
in the MYRRHA Pool	401
Results of the Second Phase of Calculations Relevant to the WPPT Benchmark on Beam Interruptions	411

TECHNICAL S	ESSION IV: SAFETY AND CONTROL OF ADS	423
	CHAIRS: J-M. LAGNIEL, P. CODDINGTON	
	P. Coddington, K. Mikityuk, M. Schikorr, W. Maschek, R. Sehgal, J. Champigny, L. Mansani, P. Meloni, H. Wider Safety Analysis of the EU PDS-XADS Designs	425
	X-N. Chen, T. Suzuki, A. Rineiski, C. Matzerath-Boccaccini, E. Wiegner, W. Maschek Comparative Transient Analyses of Accelerator-driven Systems with Mixed Oxide and Advanced Fertile-free Fuels	439
	P. Coddington, K. Mikityuk, R. Chawla Comparative Transient Analysis of Pb/Bi and Gas-cooled XADS Concepts	453
	B.R. Sehgal, W.M. Ma, A. Karbojian Thermal-hydraulic Experiments on the TALL LBE Test Facility	465
	K. Nishihara, H. Oigawa Analysis of Lead-bismuth Eutectic Flowing into Beam Duct	477
	P.M. Bokov, D. Ridikas, I.S. Slessarev On the Supplementary Feedback Effect Specific for Accelerator-coupled Systems (ACS)	485
	W. Haeck, H. Aït Abderrahim, C. Wagemans K _{eff} and K _s Burn-up Swing Compensation in MYRRHA	495
TECHNICAL S	ESSION V: ADS EXPERIMENTS AND TEST FACILITIES	505
	CHAIRS: P. D'HONDT, V. BHATNAGAR	
	H. Oigawa, T. Sasa, K. Kikuchi, K. Nishihara, Y. Kurata, M. Umeno, K. Tsujimoto, S. Saito, M. Futakawa, M. Mizumoto, H. Takano Concept of Transmutation Experimental Facility	507
	M. Hron, M. Mikisek, I. Peka, P. Hosnedl Experimental Verification of Selected Transmutation Technology and Materials for Basic Components of a Demonstration Transmuter with Liquid Fuel Based on Molten Fluorides (Development of New Technologies for Nuclear Incineration of PWR Spent Fuel in the Czech Republic)	
	Y. Kim, T-Y. Song Application of the HYPER System to the DUPIC Fuel Cycle	529
	M. Plaschy, S. Pelloni, P. Coddington, R. Chawla, G. Rimpault, F. Mellier Numerical Comparisons Between Neutronic Characteristics of MUSE4 Configurations and XADS-type Models	539

	B-S. Lee, Y. Kim, J-H. Lee, T-Y. Song Thermal Stability of the U-Zr Fuel and its Interfacial Reaction with Lead	549
SUMMARIES (OF TECHNICAL SESSIONS	557
	CHAIRS: R. SHEFFIELD, B-H. CHOI	
	Chairs: A.C. Mueller, P. Pierini Summary of Technical Session I: Accelerator Reliability	559
	Chairs: X. Cheng, T-Y. Song Summary of Technical Session II: Target, Window and Coolant Technology	565
	Chairs: W. Gudowski, H. Oigawa Summary of Technical Session III: Subcritical System Design and ADS Simulations	571
	Chairs: J-M. Lagniel, P. Coddington Summary of Technical Session IV: Safety and Control of ADS	575
	Chairs: P. D'hondt, V. Bhatagnar Summary of Technical Session V: ADS Experiments and Test Facilities	577
SUMMARIES (OF WORKING GROUP DISCUSSION SESSIONS	581
	CHAIRS: R. SHEFFIELD, B-H. CHOI	
	Chair: P.K. Sigg Summary of Working Group Discussion on Accelerators	583
	Chair: W. Gudowski Summary of Working Group Discussion on Subcritical Systems and Interface Engineering	587
	Chair: P. Coddington Summary of Working Group Discussion on Safety and Control of ADS	591
Annex 1: List of	workshop organisers	595
Annex 2: List of	participants	597



From:

Utilisation and Reliability of High Power Proton Accelerators

Workshop Proceedings, Daejeon, Republic of Korea, 16-19 May 2004

Access the complete publication at:

https://doi.org/10.1787/9789264013810-en

Please cite this chapter as:

Roelofs, Ferry, et al. (2006), "CFD Analysis of the Heavy Liquid Metal Flow Field in the MYRRHA Pool", in OECD/Nuclear Energy Agency, *Utilisation and Reliability of High Power Proton Accelerators: Workshop Proceedings, Daejeon, Republic of Korea, 16-19 May 2004*, OECD Publishing, Paris.

DOI: https://doi.org/10.1787/9789264013810-42-en

This document, as well as any data and map included herein, are without prejudice to the status of or sovereignty over any territory, to the delimitation of international frontiers and boundaries and to the name of any territory, city or area. Extracts from publications may be subject to additional disclaimers, which are set out in the complete version of the publication, available at the link provided.

The use of this work, whether digital or print, is governed by the Terms and Conditions to be found at http://www.oecd.org/termsandconditions.

